# An inviscid analysis of the Prandtl azimuthal mass-transport during swirl-type sloshing

**Odd M. Faltinsen[1]† and Alexander N. Timokha[1,2]**

[1]Centre for Autonomous Marine Operations and Systems & Department of Marine Technology, Norwegian University of Science and Technology, NO-7491 Trondheim, Norway

[2]Institute of Mathematics, National Academy of Sciences of Ukraine, 01004 Kiev, Ukraine

(Received xx; revised xx; accepted xx)

An *inviscid analytical* theory of a slow steady liquid-mass rotation during the swirl-type sloshing in a vertical circular cylindrical tank with a fairly deep depth is proposed by utilising the asymptotic steady-state wave solution by Faltinsen *et al.* (2016). The tank performs a periodic horizontal motion with the forcing frequency close to the lowest natural sloshing frequency. The azimuthal mass-transport (first observed in experiments by Prandtl 1949) is associated with the summarised effect of a *vortical* Eulerian-mean flow, which, as we show, is governed by the inviscid Craik-Leibovich equation, and an azimuthal *non*-Eulerian mean. Suggesting the mass-transport velocity tends to zero when approaching the vertical wall (supported by existing experiments) leads to a unique non-trivial solution of the Craik-Leibovich boundary problem and, thereby, gives an analytical expression for the summarised mass-transport velocity within the framework of the inviscid hydrodynamic model. The analytical solution is validated by comparing it with suitable experimental data.

## 1. Introduction

Prandtl (1949) was probably the first to demonstrate experimentally a slow steady rotation of the contained liquid during the swirl-type sloshing in an upright circular tank exposed to an orbital horizontal translatory excitation (swirl-type sloshing = *swirling* = azimuthally-propagating wave; see, Chap. 9 by Faltinsen & Timokha 2009). The azimuthal liquid mass-transport was further observed and measured by Hutton (1964) and Royon-Lebeaud *et al.* (2007) who suggested that its theoretical description should involve the Lagrangian-mean concept, in general, and the Stokes drift (which is an element of the concept, see, Craik 1986; Bühler 2009; Bremer & Breivik 2017), in particular, as well as one should account for the free-surface nonlinearity and viscosity. Recent experiments by Reclari (2013), Reclari *et al.* (2014), Ducci & Weheliye (2014), and Bouvard *et al.* (2017) paid an insight into the Prandtl phenomenon, for both almost inviscid and strongly viscous liquids (Bouvard *et al.* 2017, conducted model tests with silicon oils), to show that viscosity does not qualitatively matter, at least, when the forcing frequency is close to the lowest natural sloshing frequency, but it affects both a local vortical flow in a neighbourhood of the moving contact line and the boundary layer flow along the tank wall. However, the free-surface nonlinearity cannot be neglected at the resonance conditions.

Existing experimental works report that the mass-transport (a) is co-directed with swirl-type sloshing in each inner point beneath the free surface, (b) tends to zero when

† Email address for correspondence: odd.faltinsen@ntnu.no

approaching the upright wall, (c) reaches the maximum value at approximately the semi-radius, and (d) is satisfactorily predicted by the Stokes drift only in a neighbourhood of the tank axis. The peculiarities (a)-(d) require to account for a non-zero Eulerian-mean (vortical) velocity $\boldsymbol{w}^E$, whose appearance was extensively discussed, but not analysed in the aforementioned works by Bouvard *et al.* (2017), Reclari (2013), Reclari *et al.* (2014), Ducci & Weheliye (2014). The governing equations for $\boldsymbol{w}^E$ are the starting point of the present paper.

In § 2, we introduce the steady-state potential-flow Narimanov-Moiseev–type solution by Faltinsen *et al.* (2016) describing the steady-state resonant sloshing in an upright circular tank, which is horizontally excited with the forcing frequency close to the lowest natural sloshing frequency. The lowest-order component of this solution is determined by the four lowest-order amplitude parameters $a, \bar{a}, \bar{b}$ and $b$. As follows from Faltinsen *et al.* (2016), one can introduce the nondimensional parameter $\Xi = ab - \bar{b}\bar{a}$ whose sign determines the existing steady-state wave types: standing ($\Xi = 0$), counter- ($\Xi > 0$) and clockwise ($\Xi < 0$) swirling waves (azimuthal progressive wave). In a frequency range, the steady-state sloshing can be unstable that causes chaotic (irregular) wave motions. Limitations of the steady-state solution are discussed.

In § 3, the Eulerian-mean (vortical) flow velocity $\boldsymbol{w}^E$ is added to the second-order asymptotic component of the steady-state solution by Faltinsen *et al.* (2016). The time-averaging in the vorticity equation derives the dynamic governing equation for $\boldsymbol{w}^E$, which is the same as the inviscid Craik-Leibovich equation (Craik & Leibovich 1976). In § 4, we evaluate the mean azimuthal mass-flux $M = M^E + M^s$, where $M^E$ is caused by $\boldsymbol{w}^E$, but the second summand $M^s$, which is not zero for swirling, is in the standard way interpreted as a consequence of the non-Eulerian azimuthal (Stokes-drift–type) mass-transport velocity $\boldsymbol{w}^s$. Mathematical and physical reasons for the difference between $\boldsymbol{w}^s$ (and $M^s$) and the formal mathematical expression of the Stokes drift velocity $\boldsymbol{w}^S$ (and the associated mass-flux $M^S$) are discussed. In the forthcoming analysis, the experimentally-established mass-transport is associated with the sum $\boldsymbol{w}^P = \boldsymbol{w}^E + \boldsymbol{w}^s$.

Along with the inviscid Craick-Leibovich equation, the steady solenoidal $\boldsymbol{w}^E$ satisfies the zero normal-velocity conditions on the wall and the mean free surface. Getting a unique $\boldsymbol{w}^E$ requires tangential (azimuthal and vertical) boundary conditions on the wetted tank surface. An indicative prediction of these conditions can be obtained by using the nonlinear boundary layer (steady streaming) theory whose details are described in the Supplementary Materials B. Analysis of these predictions in § 5 shows that they are mathematically contradictory. However, a much more important fact is that they do not provide the zero mass-transport velocity $\boldsymbol{w}^P = \boldsymbol{0}$ on the wetted tank wall, which was listed above as the peculiarity (b). A physical reason is that the Eulerian steady streaming theory ignores the non-Eulerian mass-transport (associated with $\boldsymbol{w}^s$) around the wall, which influences viscous stresses and may modify tangential boundary conditions.

By assuming that the non-Eulerian mass-transport predominates the local tangential mean rotation of fluid particles in a neighbourhood of the wall, one can arrive, in the inviscid flow limit, at the tangential boundary condition $\boldsymbol{w}^P = \boldsymbol{0} \Rightarrow \boldsymbol{w}^E = -\boldsymbol{w}^s$ on the wall. The latter condition makes the experimental peculiarity (b) automatically satisfied. It also means that $\boldsymbol{w}^E$ counteracts $\boldsymbol{w}^s$ and, thereby, implies the return flow. Adopting this boundary condition makes the *inviscid* Craik-Leibovich boundary value problem mathematically correct and allows for deriving an exact analytical solution for $\boldsymbol{w}^P$. As announced in the paper title, this purely *inviscid* solution neglects specific viscous streams and their influence (feedback) on the Prandtl phenomenon. The inviscid approximation of the azimuthal mass-transport is validated in § 6 by using the measurements by Hutton (1964) and Bouvard *et al.* (2017).

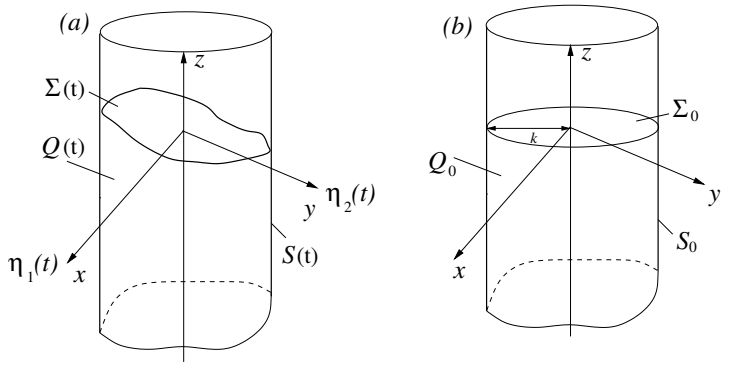


FIGURE 1. The upright circular container with an infinite liquid depth moves translatory along an horizontal elliptic orbit defined by $\eta_1(t) = \eta_{1a}\cos\sigma t$, $\eta_2(t) = \eta_{2a}\sin\sigma t$. Sloshing is considered in the tank-fixed coordinate system. The panel (a) introduces the original geometric notations but (b) shows the mean (hydrostatic) liquid domain $Q_0$, unperturbed free surface $\Sigma_0$ and the mean wetted tank surface $S_0$ as they appear in our nondimensional analysis.

## 2. Steady-state asymptotic solution by Faltinsen *et al.* (2016)

A rigid circular cylindrical container of radius $r_0$ is partly filled by an inviscid incompressible liquid with a fairly deep depth (figure 1, a). Liquid sloshing is considered in the tank-fixed cylindrical coordinate system. The tank performs an orbital (longitudinal, elliptic, or circular) small-magnitude horizontal translatory motion governed by $\eta_1(t) = \eta_{1a}\cos\sigma t$, $\eta_2(t) = \eta_{2a}\sin\sigma t$ along the $x$ and $y$ axes, respectively. The forcing frequency $\sigma$ is close to the lowest natural sloshing frequency $\sigma_1 = \sigma_{11}$. For the infinite liquid depth, the natural sloshing frequencies are $\sigma_{Mi} = \sqrt{gk_{Mi}/r_0}$, where $g$ is the gravity acceleration and $k_{Mi}$ are the roots of $J'_M(k_{Mi}) = 0$ ($J_M$ is the Bessel function of the first kind).

Assuming irrotational flows of an incompressible perfect liquid, Faltinsen *et al.* (2016) derived an asymptotic steady-state solution of the nonlinear resonant sloshing problem for finite deep liquid depths $h$ ($1.2 \lesssim h^* = h/r_0$). The derivations were based on the Narimanov-Moiseev asymptotic multimodal theory, which is a consequence of the Bateman-Luke variational formalism for the free-surface sloshing problem coupling the velocity potential $\varphi(r,\theta,z,t)$ and function $\zeta(r,\theta,t)$ describing the free-surface elevations by $z = \zeta(r,\theta,t)$. The constructed asymptotic solution by Faltinsen *et al.* (2016) exactly satisfies the Laplace equation, boundary conditions on the wetted tank walls, but kinematic and dynamic boundary conditions on the free surface $\Sigma(t)$ are asymptotically approximated within to the $o(\epsilon)$-terms, where the lowest-order surface wave component has then the order $O(\epsilon^{1/3})$ and the highest included asymptotic terms $O(\epsilon) \ll 1$ are associated with the nondimenional forcing amplitudes. Why the steady-state resonant sloshing amplitude is of the order $O(\epsilon^{1/3})$ while the tank amplitude is of the order $O(\epsilon)$ was explained by Moiseev (1958) (see also details in chapters 8 and 9 by Faltinsen & Timokha 2009).

We utilise the steady-state asymptotic solution by Faltinsen *et al.* (2016) for $h^* \to \infty$ and re-write it with special normalisation, in which $1/\sigma$ and $r_0/k$ are characteristic time and length, respectively, ($k = k_{11} = 1.841183781341...$). This normalisation simplifies the forthcoming derivations and analytical expressions. The lowest-order terms in the asymptotic free-surface $\Sigma(t)$ representation,

$$z = \zeta(r,\theta,t) = \zeta^{(1/3)}(r,\theta,t) + \zeta^{(2/3)}(r,\theta,t) + \zeta^{(3/3)}(r,\theta,t) + ...,$$

take then the form

$$\zeta(r,\theta,t)=\zeta^{(1/3)}(r,\theta,t)+o(\epsilon^{1/3})=J_1(r)\,(-\theta_s\cos t+\theta_c\sin t)+o(\epsilon^{1/3}), \tag{2.1}$$

where

$$\theta_c=\theta_c(\theta)=b\sin\theta+\bar{a}\cos\theta,\quad \theta_s=\theta_s(\theta)=-\bar{b}\sin\theta-a\cos\theta$$

and $a,\bar{a},\bar{b},b=O(\epsilon^{1/3})$ are the *only* lowest-order nondimensional amplitude parameters. The asymptotic velocity field *relative* to the rigid tank is defined by

$$\boldsymbol{v}(r,\theta,z,t)=v_1\hat{\boldsymbol{r}}+v_2\hat{\boldsymbol{\theta}}+v_3\hat{\boldsymbol{z}}=\boldsymbol{v}^{(1/3)}+\boldsymbol{v}^{(2/3)}+\boldsymbol{v}^{(3/3)}+..., \tag{2.2}$$

where $\hat{\boldsymbol{r}},\hat{\boldsymbol{\theta}},\hat{\boldsymbol{z}}$ are the unit vectors in the cylindrical coordinate frame. The lowest-order potential-flow velocity component is

$$\begin{aligned}\boldsymbol{v}^{(1/3)}(r,\theta,z,t)&=\nabla\left[J_1(r)\,e^z\,(\theta_c\cos t+\theta_s\sin t)\right]\\&=\left[J_1'(r)e^z\,(\theta_c\cos t+\theta_s\sin t)\right]\hat{\boldsymbol{r}}+\left[r^{-1}J_1(r)e^z\,(\theta_c'\cos t+\theta_s'\sin t)\right]\hat{\boldsymbol{\theta}}\\&\quad+\left[J_1(r)e^z\,(\theta_c\cos t+\theta_s\sin t)\right]\hat{\boldsymbol{z}}=v_1^{(1/3)}\hat{\boldsymbol{r}}+v_2^{(1/3)}\hat{\boldsymbol{\theta}}+v_3^{(1/3)}\hat{\boldsymbol{z}},\end{aligned} \tag{2.3}$$

where the velocity potential $\varphi^{(1/3)}(r,\theta,z)=J_1(r)\,e^z\,(\theta_c\cos t+\theta_s\sin t)$ is taken from Faltinsen *et al.* (2016) and $\theta_c'$, $\theta_s'$ are derivatives of $\theta_c$, $\theta_s$ by $\theta$. The relative velocity component $\boldsymbol{v}^{(1/3)}$ is constructed in the body-fixed coordinate system and, therefore, it satisfies the impermeability condition on the wetted tank surface as well as the kinematic and dynamic free-surface boundary conditions (see, details in chapters 2 and 5 by Faltinsen & Timokha 2009).

Depending on the quadratic amplitude quantity $\Xi=ab-\bar{a}\bar{b}$, the free-surface representation (2.1) determines either standing (only possible for longitudinal horizontal excitations) or swirling (azimuthal progressive) wave, i.e.

$$\Xi=0\Leftrightarrow\text{standing};\ \Xi>0\Leftrightarrow\text{counterclockwise swirl};\ \Xi<0\Leftrightarrow\text{clockwise swirl}. \tag{2.4}$$

We construct an *inviscid vortical* asymptotic solution for the swirl-type sloshing, in which the lowest-order velocity field coincides with (2.3) but a steady vorticity appears in the second-order approximation, $O(\epsilon^{2/3})$. Owing to restrictions of the Narimanov-Moseev asymptotic theory, proceeding this way implicitly assumes:

(i) the low-viscous contained liquid, for which the boundary layer-thickness at the tank wall, $\delta=1/\sqrt{Re_s}\ll 1$ ($Re_s=(r_0^2\sigma)/(\nu k)$, is the sloshing-related Reynolds number and $\nu$ is the kinematic viscosity) is smaller than the introduced steady vortical component, i.e.,

$$\delta=\frac{1}{\sqrt{Re_s}}=\sqrt{\frac{\nu k}{r_0^2\sigma}}\ll O(\epsilon^{2/3}); \tag{2.5}$$

(ii) the fairly deep liquid depth (practically, $2.5\lesssim h^*=h/r_0$ to avoid the depth effect on the natural sloshing frequencies);

(iii) the forcing frequency $\sigma$ is close to the lowest natural sloshing frequency $\sigma_1=\sigma_{11}$, so that the Moiseev detuning condition

$$(\sigma_1^2/\sigma^2-1)=O(\epsilon^{2/3}),\quad k\sqrt{\eta_{1a}^2+\eta_{1a}^2}/r_0=O(\epsilon)\ll 1 \tag{2.6}$$

is satisfied, namely, the closeness of the forcing frequency $\sigma$ to the first natural sloshing frequency $\sigma_1$ is measured on the $O(\epsilon^{2/3})$-scale, where $O(\epsilon)$ characterises the forcing amplitude;

(iv) there are no secondary resonances, which occur, e.g., in local neighbourhoods

of $\sigma/\sigma_1 = \sigma_{2k}/(2\sigma_1), \sigma/\sigma_1 = \sigma_{0k}/(2\sigma_1), \sigma/\sigma_1 = \sigma_{3k}/(3\sigma_1)$, $k \geqslant 1$ and $\sigma/\sigma_1 = \sigma_{1i}/(3\sigma_1)$, $i \geqslant 2$ (the secondary resonances were extensively discussed by Faltinsen *et al.* 2016).

*Remark.* Faltinsen *et al.* (2016, Eq. (3.12)) derived a system of nonlinear algebraic secular (solvability) equations governing $a, \bar{a}, \bar{b}$ and $b$ as functions of $\sigma/\sigma_1$. The secular system comes from the third-order ($O(\epsilon)$) approximation and, therefore, its coefficients can modify due to the introduced second-order vortical component. However, structure of (2.1) and (2.3) remains the same and, therefore, we can assume that $a, \bar{a}, \bar{b}, b$ are the known amplitude values, but not necessarily the same as computed by Faltinsen *et al.* (2016). How $a, \bar{a}, \bar{b}, b$ change due to the non-zero vortical flow deserves a dedicated study.

## 3. The Eulerian-mean velocity field

The original asymptotic solution by Faltinsen *et al.* (2016) implies the zero mean velocity field. In the present section, we assume that, after a long, and, generally, viscous-flow transient wave phase, the velocity field became vortical so that the steady-state solution contains the non-zero time-averaged (Eulerian-mean) solenoidal velocity component

$$\begin{aligned} &\langle \boldsymbol{v} \rangle = \boldsymbol{w}^E(r,\theta,z) = (w_1^E, w_2^E, w_3^E) = O(\epsilon^{2/3}), \\ &\langle \nabla \times \boldsymbol{v} \rangle = \nabla \times \boldsymbol{w}^E = \boldsymbol{\Omega}^E(r,\theta,z) = (\Omega_1^E, \Omega_2^E, \Omega_3^E) \neq \boldsymbol{0}, \end{aligned} \tag{3.1}$$

such that

$$\nabla \cdot \boldsymbol{w}^E = 0; \quad \nabla \cdot \boldsymbol{\Omega}^E = \nabla \cdot [\nabla \times \boldsymbol{w}^E] \equiv 0. \tag{3.2}$$

This velocity component is associated with the following framed *second-order supplement* to the original asymptotic solution

$$\boldsymbol{v}^{(2/3)}(r,\theta,z,t) = \boxed{\boldsymbol{w}^E(r,\theta,z)} + \nabla\varphi_{2/3}^{\cos}(r,\theta,z)\cos 2t + \nabla\varphi_{2/3}^{\sin}(r,\theta,z)\sin 2t. \tag{3.3}$$

To get a governing (dynamic) equation for $\boldsymbol{w}^E$, we follow the asymptotic (time-averaging) procedure by Craik & Leibovich (1976) (not that in Leibovich 1980). The procedure uses the vorticity equation written down in the tank-fixed (non-inertial) coordinate frame (see, Kochin *et al.* 1965; Faltinsen & Timokha 2009),

$$\dot{\boldsymbol{\Omega}} = \nabla \times [(\boldsymbol{v} - \boldsymbol{v}_O) \times \boldsymbol{\Omega}], \quad \boldsymbol{\Omega} = \nabla \times \boldsymbol{v}, \tag{3.4}$$

where $\boldsymbol{v}_O = k(\dot{\eta}_1(t), \dot{\eta}_2(t), 0)/(r_0\sigma) = O(\epsilon)$ is the nondimensional translatory velocity of the tank, which appears in (3.4) because we employ the non-inertial coordinate system, and the dot means differentiation by the time. The time-periodic solution of (3.4) is asymptotically posed as

$$\boldsymbol{\Omega} = \boldsymbol{\Omega}^E + \boldsymbol{\Omega}_{3/3} + \boldsymbol{\Omega}_{4/3} + \dots\,; \;\; \boldsymbol{v} = \boldsymbol{v}^{(1/3)} + \boldsymbol{v}^{(2/3)} + \dots, \tag{3.5}$$

in which $\boldsymbol{\Omega}^E$ is defined in (3.1), $\boldsymbol{v}^{(1/3)}$ comes from (2.3), $\boldsymbol{v}^{(2/3)}$ contains the vortical term by (3.3)

Substituting (3.5) into the vorticity equation (3.4) derives the time-periodic (3/3)-order approximation

$$\begin{aligned} \boldsymbol{\Omega}_{3/3}(r,\theta,z,t) &= \int \nabla \times \left[\boldsymbol{v}^{(1/3)} \times \boldsymbol{\Omega}^E\right] \mathrm{d}t \\ &= \nabla \times \left[\nabla(J_1\theta_c e^z) \times \boldsymbol{\Omega}^E\right] \sin t - \nabla \times \left[\nabla(J_1\theta_s e^z) \times \boldsymbol{\Omega}^E\right] \cos t. \end{aligned} \tag{3.6}$$

The (4/3)-order asymptotic approximation of the vorticity equation

$$\dot{\boldsymbol{\Omega}}_{4/3} = \nabla \times [\boldsymbol{w}^E \times \boldsymbol{\Omega}^E] + \nabla \times [\boldsymbol{v}^{(1/3)} \times \boldsymbol{\Omega}_{3/3}] \tag{3.7}$$

leads to the time-periodic solution $\boldsymbol{\Omega}_{4/3}$, if and only if, the time-averaged right-hand side of (3.7) is zero. Tedious derivations (we used Maple$^{TM}$ to simplify them) show that, if $\boldsymbol{\Omega}^E$ is solenoidal (satisfies (3.2)), the time-averaging in (3.7) yields the following equation

$$\nabla \times [\boldsymbol{w}^E \times \boldsymbol{\Omega}^E] = \Xi\, e^{2z}\left(\frac{1}{r} w^S\, \partial_\theta \boldsymbol{\Omega}^E - \hat{\boldsymbol{\theta}}\left[\underbrace{\left((w^S)' - \frac{1}{r} w^S\right)}_{3r^{-1}(-2w^S + w^s)} \Omega_1^E + 2 w^S\, \Omega_3^E\right]\right), \tag{3.8}$$

where $w^s(r) = r^{-1} J_1^2(r)$ and $w^S(r)$ is associated with the formally-defined *Stokes drift velocity*†

$$\boldsymbol{w}^S(r,z) \stackrel{\text{def}}{=} \left\langle \int \boldsymbol{v}^{(1/3)} \mathrm{d}t \cdot \nabla \boldsymbol{v}^{(1/3)} \right\rangle = \frac{1}{2} \nabla \times \left\langle \boldsymbol{v}^{(1/3)} \times \int \boldsymbol{v}^{(1/3)} \mathrm{d}t \right\rangle$$
$$\equiv \Xi e^{2z} \underbrace{\frac{1}{2r}\left[J_1^2(r) + \left(J_1' - \frac{J_1(r)}{r}\right)^2\right]}_{w^S(r)} \hat{\boldsymbol{\theta}} = w_2^S(r,z)\hat{\boldsymbol{\theta}}. \tag{3.9}$$

The derived equation (3.8) is the same as the *inviscid Craik-Leibovich equation* (Craik & Leibovich 1976) but for swirling, that is, (3.8) admits the well-known equivalent form

$$\nabla \times [\underbrace{(\boldsymbol{w}^E + \boldsymbol{w}^S)}_{\boldsymbol{w}^L} \times \boldsymbol{\Omega}^E] = \boldsymbol{0}. \tag{3.10}$$

Equivalence of (3.10) and (3.8) is shown in the Supplementary Materials A.

The governing equations (3.2) and (3.8) with respect to $\boldsymbol{w}^E$ require appropriate boundary conditions, which include, since we employ the tank-fixed coordinate system, the zero normal velocity conditions on the wall and the mean free surface

$$w_1^E(k,\theta,z) = 0 \quad \text{and} \quad w_3^E(r,\theta,0) = 0, \tag{3.11}$$

as well as

$$|\boldsymbol{w}^E| \to 0 \quad \text{as} \quad z \to -\infty. \tag{3.12}$$

However, (3.2) and (3.8) also need *tangential* boundary conditions on the wetted wall. Where the tangential boundary conditions for the *inviscid* velocity field $\boldsymbol{w}^E$ could come from is analysed in § 5.

## 4. The mean mass-transport through the meridional plane

Let us forget, for a while, derivations in the previous section but assume that we know the axisymmetric *time-averaged Eulerian* (vortical) velocity by (3.1) in each inner point of the time-dependent liquid domain, i.e.,

$$\boldsymbol{w}^E(r,z) = \langle \boldsymbol{v} \rangle + o(\epsilon^{2/3}), \tag{4.1}$$

which has already appeared in (3.3). The lowest-order free-surface motion $\zeta^{(1/3)}$ and velocity field $v^{(1/3)}$ are described by (2.1) and (2.3), respectively.

Simple derivations show that the mean mass-flux through the horizontal on $z = z_1 < 0$

† We thank Dr. Herreman who prompted using the second definition of the Stokes drift.

and annular $r = r_1$, $0 < r_1 < k$ cross-sections are zeros (physically, due to the liquid mass conservation). However, the integral mass-transport (mass-flux) through the meridional cross-section (in the $\hat{\boldsymbol{\theta}}$ direction) is not zero and reads as

$$M = \left\langle \int_{-\infty}^{\zeta^{(1/3)}(r,\theta,t)} \int_0^k \left( v_2^{(1/3)} + v_2^{(2/3)} \right) \mathrm{d}r\mathrm{d}z \right\rangle + o(\epsilon^{2/3}), \tag{4.2}$$

where $v^{(2/3)}$ is defined by (3.3).

The asymptotic series in (4.2) shows that

$$M = \underbrace{\int_{-\infty}^{0} \int_0^k w_2^E(r,z)\,\mathrm{d}r}_{M^E} + \underbrace{\int_0^k \left\langle v_2^{(1/3)}|_{z=0}\, \zeta^{(1/3)} \right\rangle}_{M^s} + o(\epsilon^{2/3}) \tag{4.3}$$

where $M^E$ implies the Eulerian-mean azimuthal mass-flux but the second mass-flux contribution, $M^s$, does *not* depend on $\boldsymbol{w}^E$, but is a consequence of a quadratic quantity by the lowest-order potential-flow terms. Following derivations by Faltinsen & Timokha (2009, Sect. 9.6.3) gives

$$M^s = \int_0^k \left\langle \left[ v_2^{(1/3)} \int v_3^{(1/3)} \mathrm{d}t \right]_{z=0} \right\rangle \mathrm{d}r + o(\epsilon^{2/3}) = \tfrac{1}{2}\Xi \int_0^k \frac{J_1^2(r)}{r} \mathrm{d}r + o(\epsilon^{2/3}), \tag{4.4}$$

which shows that $M^s \neq 0$ for swirling ($\Xi \neq 0$).

Derivations in (4.4) utilised the linear kinematic boundary condition on the free surface $\dot{\zeta}^{(1/3)} = v_3^{(1/3)}|_{z=0}$. This boundary condition states that the fluid particles on the free surface move together with this surface and, in particular, $\zeta^{(1/3)} = d_3^{(1/3)}|_{z=0}$, where

$$\boldsymbol{d}^{(1/3)} = (d_1^{(1/3)}, d_2^{(1/3)}, d_3^{(1/3)}) = \int \boldsymbol{v}^{(1/3)} \mathrm{d}t$$

is the first order Lagrangian displacements. The *dual Eulerian-Lagrangian character* of the wave elevation $\zeta^{(1/3)} = d_3^{(1/3)}$ makes it possible to interpret $M^s$ in (4.3) as being caused by the Stokes-drift–type mass-transport. This resolves the mathematical paradox – the extra non-zero contribution $M^s$ into the total mass-flux $M$, which is formally computed within the framework of the Eulerian specification and, therefore, should be equal to $M^E$.

Treatment of the non-zero integrals alike $M^s$ as coming from the non-Eulerian mean component of the mass-transport is *typical* for the external progressive surface-wave problems. Details and discussions can be found in books and review papers, which are exemplified by Bühler (2009) and Bremer & Breivik (2017). Pursuing a self-contained presentation, we add an illustrative example in the Supplementary Materials C where the link between the Stokes-drift mass-flux and an integral alike $M^s$ is shown for progressive waves in a rectangular channel by using the Stokes integration theorem and (3.9).†

By adopting definition (3.9) of the Stokes drift velocity $\boldsymbol{w}^S$, we can examine whether the latter fact from the external surface wave theory remains correct for the studied problem. For this purpose, we consider the integral over the azimuthal Stokes-drift velocity and apply the Stokes integration theorem:

$$M^S = \int_{-\infty}^{0} \int_0^k w_2^S(r,z)\mathrm{d}r\mathrm{d}z = \frac{1}{2} \int_{-\infty}^{0} \int_0^k \left( \nabla \times \left\langle \boldsymbol{v}^{(1/3)} \times \int \boldsymbol{v}^{(1/3)} \mathrm{d}t \right\rangle \right) \cdot \hat{\boldsymbol{\theta}}\, \mathrm{d}r\mathrm{d}z$$

† The idea of using (3.9) is proposed by Dr. W. Herreman.

$$= \frac{1}{2}\int_{-\infty}^{0}\left\langle v_1^{(1/3)}\int v_2^{(1/3)}\mathrm{d}t - v_2^{(1/3)}\int v_1^{(1/3)}\mathrm{d}t\right\rangle\Big|_{r\to 0}\mathrm{d}z$$
$$+\frac{1}{2}\int_{0}^{k}\left\langle v_2^{(1/3)}\int v_3^{(1/3)}\mathrm{d}t - v_3^{(1/3)}\int v_2^{(1/3)}\mathrm{d}t\right\rangle\Big|_{z=0}\mathrm{d}r$$
$$+\frac{1}{2}\int_{0}^{-\infty}\left\langle v_1^{(1/3)}\int v_2^{(1/3)}\mathrm{d}t - v_2^{(1/3)}\int v_1^{(1/3)}\mathrm{d}t\right\rangle\Big|_{r=k}\mathrm{d}z$$
$$+\frac{1}{2}\int_{k}^{0}\left\langle v_2^{(1/3)}\int v_3^{(1/3)}\mathrm{d}t - v_3^{(1/3)}\int v_3^{(1/3)}\mathrm{d}t\right\rangle\Big|_{z\to-\infty}\mathrm{d}r. \quad (4.5)$$

Here, the third and fourth integrals are zeros but the first one implies the limit $-\frac{1}{4}\Xi[J_1'(r)J_1(r)r^{-1}] \to -\frac{1}{16}\Xi$ as $r\to 0$.

Because

$$\left\langle v_3^{(1/3)}\int v_2^{(1/3)}\right\rangle\Big|_{z=0} = -\left\langle v_2^{(1/3)}\int v_3^{(1/3)}\right\rangle\Big|_{z=0};$$
$$\left\langle v_1^{(1/3)}\int v_2^{(1/3)}\right\rangle\Big|_{r\to 0} = -\left\langle v_2^{(1/3)}\int v_1^{(1/3)}\right\rangle\Big|_{r\to 0},$$

the derivation line (4.5) results in

$$\underbrace{\int_0^k\left\langle v_2^{(1/3)}|_{z=0}\,\zeta^{(1/3)}\right\rangle}_{M^s} = M^S + \underbrace{\int_{-\infty}^{0}\left\langle v_2^{(1/3)}d_1^{(1/3)}\right\rangle\Big|_{r\to 0}\mathrm{d}z}_{\frac{1}{16}\Xi}, \quad (4.6)$$

where $d_1^{(1/3)}|_{r\to 0} = \int v_1^{(1/3)}\mathrm{d}t|_{r\to 0}$ expresses the first-order radial Lagrangian displacement for fluid particles, which belong (but do not cross the tank axis) to a meridional plane $\theta=\theta_0$=const as $r\to 0$.

Formula (4.6) links the actual non-Eulerian mean mass-flux $M^s$ and its formal mathematic prediction based on the Stokes mass-transport concept, $M^S$. The formula and derivation line (4.5) also helps to clarify the difference between $M^s$ and $M^S$. Computing $M^S$ *ignores* the fluid particles in the meridional plane and their first-order Lagrange displacements, which cross the tank centre, namely, the fluid particles, which move between in the meridional plane $\theta=\theta_0$=const and the meridional plane $\theta=\theta_0+\pi$. In the contrast, $M^s$ determines the azimuthal *mass-flux as it stands*, including the effect of these cross-moving particles.

One can rebuild (extract)

$$\boldsymbol{w}^s(r,z) = w_2^s(r,z)\,\hat{\boldsymbol{\theta}}, \quad M^s = \int_{-\infty}^{0}\int_0^k w_2^s(r,z)\,\mathrm{d}r\mathrm{d}z,$$

which would plays the same role as the Stokes drift velocity $\boldsymbol{w}^S$ for the external progressive waves. For this purpose, we replace the finite integration on $(0,k)$ in (4.4) by a small interval $(r, r+\Delta r)$ that gives, in the limit $\Delta r\to 0$, that $w_2^s(r,z) = \Xi F(z)\,r^{-1}\,J_1^2(r)$. To derive $F(z)$, one should exclude integration by $r$ in (4.4), fix the radial coordinate $0<r=r_0<k$ and consider integration by $z$ from $-\infty$ to $d_3^{(1/3}|_{z=z_0} = \zeta_{z_0} = e^{z_0}\int v_3^{(1/3)}(r_0,\theta,z_0)\mathrm{d}t + o(\epsilon^{1/3})$ in (4.4), where $-\infty<z_0<0$ is a fixed vertical coordinate in the mean cross-sectional area. This gives $\int_{-\infty}^{z_0}F(z)dz = \frac{1}{2}e^{2z_0}$ and, therefore, $F(z)=e^{2z}$. As a consequence,

$$\boldsymbol{w}^s(r,z) = \Xi e^{2z}w^s(r)\hat{\boldsymbol{\theta}} = \Xi e^{2z}\frac{J_1^2(r)}{r}\hat{\boldsymbol{\theta}}, \quad (4.7)$$

where $\boldsymbol{w}^s$ has already appeared for the inviscid Craik-Leibovich equation.

In *summary*, to describe the mass-flux (4.3) in the Prandtl experiments one should consider

$$\boldsymbol{w}^P = \boldsymbol{w}^s + \boldsymbol{w}^E, \tag{4.8}$$

where $\boldsymbol{w}^s$ implies, according to the generally-accepted physical treatment of $M^s$, the non-Eulerian (Stokes-drift–type) velocity (4.7) but the Eulerian-mean velocity $\boldsymbol{w}^E$ is governed by the boundary value problem (3.2), (3.8)-(3.12) whose unique non-trivial solution requires tangential boundary conditions on the wetted tank wall.

## 5. The mass-transport velocity $\boldsymbol{w}^P$

### 5.1. *Where the tangential boundary conditions for $\boldsymbol{w}^E$ may come from?*

There are no physical mechanisms causing tangential boundary conditions for $\boldsymbol{w}^E$ by (3.2), (3.8)-(3.12) within the framework of the fully *inviscid* hydrodynamic model. Usually, the steady tangential stresses and associated boundary conditions are related to steady streaming (Riley 2001), a nonzero Eulerian-mean of fluctuating flows, which is normally, caused by the action of an oscillating submerged body, or, indirectly, by the action of viscous stresses in thin boundary layers at *no-slip* boundaries, here, at the vertical wall. The Supplementary Materials B derive the tangential boundary conditions (B 23*a*) and (B 23*b*) as they follow from the steady streaming theory for the swirl-type sloshing. These Eulerian derivations ignore the non-Eulerian mean mass-transport of fluid particles around (in a small neighbourhood of) the wall, which should, in contrast to the inner liquid points, influence the viscous stresses and, mathematically, modify no-slip conditions, which must, in addition, be applied, according to experiments, to the azimuthal mass-transport on the vertical wall. Physically, this means that moving fluid particles due to $\boldsymbol{w}^s$, when being not zero at $r = k$, cause an extra vorticity.

We have no an idea on how to include the non-zero $\boldsymbol{w}^s$, $r \to k$ into the steady streaming theory. However, we can either neglect the Stokes-drift–type mass-transport at the wall or assume that $\boldsymbol{w}^s$ predetermines the inviscid Eulerian-mean $\boldsymbol{w}^E$ so that other viscous streams lead to negligible contribution into $\boldsymbol{w}^P$.

#### 5.1.1. *Steady streaming with negligible $\boldsymbol{w}^s$ at the wall*

By ignoring the non-Eulerian mean mass-transport by $\boldsymbol{w}^s$ on the wall, the Supplementary Materials B derive the tangential boundary conditions, (B 23*a*) and (B 23*b*), which express the Eulerian-mean steady streaming. Because Faltinsen *et al.* (2016) showed that $\bar{a} = \bar{b} = 0$ and $a \approx b$ for undamped sloshing, at least, for the orbital tank forcing, one can focus on the framed terms in (B 23*a*) and (B 23*b*). Comparing (B 23*b*) with $w_3^E = 0$ on the mean free surface in (3.11) shows that using (B 23*b*) in our inviscid analysis is mathematically contradictory, because this causes $\boldsymbol{w}^E$ to be discontinuous but $\boldsymbol{\Omega}^E = \nabla \times \boldsymbol{w}^E$ becomes singular (infinite) at the contact point $r = k$, $z = 0$, and, as a consequence, asymptotic analysis in § 3 is invalid as involving the infinite function $\boldsymbol{\Omega}^E$ in the second-order approximation. This mathematical problem is well known from viscous CFD simulations. Its resolution requires to relax the no-slip condition about the moving contact line. However, existing computational approaches are not adoptable in analytical *inviscid* studies.

The azimuthal tangential boundary condition (B 23*a*) states that $\boldsymbol{w}^E$ has in each inner point the opposite sign to $\Xi$ and, therefore, $\boldsymbol{w}^E$ implies the return flow (in opposite direction to swirling). However, (B 23*a*) does not provide the experimental peculiarity

(b) consisting of the zero mass-transport on the wall, $w_2^P = 0$, $r = k$. Indeed, imposing $w_2^P = 0$ ($w_2^E = -w_2^s$) at $r = k$ gives

$$w_2^E = -\Xi e^{2z} p_0 = -\Xi e^{2z} p_0^s \text{ at } r = k, \quad p_0^s = \frac{J_1^2(k)}{k} > 0, \tag{5.1}$$

which should be compared with

$$w_2^E = -\Xi e^{2z} p_0 = -\Xi e^{2z} p_0^V \text{ at } r = k, \quad p_0^V = \frac{3(k^2-1)J_1^2(k)}{4k^3} > 0 \tag{5.2}$$

following from (B 23$a$). Calculations show that $p_0^V/p_0^s = 0.5287583024...$, and, therefore, (B 23$a$) underpredicts (almost twice) the needed value.

5.1.2. *The non-Eulerian mass-transport $\boldsymbol{w}^s$ plays a dominant role at the wall*

Assuming the dominant role of $\boldsymbol{w}^s$ at the wall is *physically* consistent with the inviscid limit, $Re_s \to \infty$, when purely viscous stresses due to *no-slip* conditions for oscillatory flow components and associated viscous steady streams may be neglected. Considering the inviscid limit and the time-averaging procedure of the no-slip conditions for the resulting particle motions around the wall make the latter conditions automatically satisfied for the $O(\epsilon^{1/3})$ asymptotic component but the $O(\epsilon^{2/3})$ approximation *mathematically* leads to the tangential boundary condition

$$\boldsymbol{w}^P = 0 \;\Rightarrow \qquad w_2^E = -\Xi e^{2z} p_0 = -\Xi e^{2z} p_0^s \quad \text{and} \quad w_3^E = 0 \;\text{ at } r = k. \tag{5.3}$$

This condition is exactly the same as required by the peculiarity (b) (see, Introduction). It means that liquid particles, which are involved into the mass-transport $\boldsymbol{w}^P$, are unmovable (do not steadily slip) along the wall but their components, $\boldsymbol{w}^s$ (non-Eulerian mean) and $\boldsymbol{w}^E$ (Eulerian mean) eliminate each other on the wetted tank surface. The Eulerian-mean implies the return flow. The mass-transport becomes self-supported when equipped with (5.3). Decreasing $\boldsymbol{w}^E$ at the wall (due to small viscous stresses) makes the mass-transport around the wall by $\boldsymbol{w}^s$ generating a tangential stresses counteracting $\boldsymbol{w}^s$ until (5.3) is fulfilled.

Usage of (5.3) is mathematically not contradictory but we should understand that this condition neglects purely viscous streams including the poloidal recirculation (details of the viscous phenomena are extensively discussed by Bouvard *et al.* 2017). This condition can also be treated as an hypothetical analogy of the Kutta-Joukowski condition applied to foils in inviscid fluid with rotational flow.

### 5.2. *The resulting mass-transport velocity*

Accepting (5.3) causes an axisymmetric solution of the boundary value problem (3.2), (3.8)-(3.12). Furthermore, if the vector-function $\boldsymbol{w}^E(r,z)$ is continuous and finite in $Q_0$, the $\hat{\boldsymbol{r}}$ and $\hat{\boldsymbol{z}}$ components of the the Craik-Leibovich equation (3.8) reduce to

$$\partial_z G = 0 \;\&\; (r\,\partial_r G + G) = 0 \quad \left(G = w_1^E \Omega_3^E - w_3^E \Omega_1^E\right) \;\Rightarrow G = G(r) = C/r \;\Rightarrow G = 0 \tag{5.4}$$

and, therefore,

$$\partial_z \left(r w_2^E\right) w_3^E + \partial_r \left(r w_2^E\right) w_1^E = 0 \;\text{ in } Q_0, \tag{5.5}$$

but (3.2) transforms to

$$\partial_z \left(r w_3^E\right) + \partial_r \left(r w_1^E\right) = 0 \;\text{ in } Q_0. \tag{5.6}$$

Eqs. (5.5), (5.6) are restricted to the homogeneous boundary conditions (3.11) and (5.3b). Because we assume a non-trivial azimuthal velocity component $w_2^E$, which appears

in coefficients of (5.5), (5.6), the boundary problem (5.5), (5.6), (3.11), (5.3b) can be solved by using, e.g., method of characteristics, which leads to the trivial solution $w_1^E = w_3^E \equiv 0$.

The $\hat{\boldsymbol{\theta}}$-component of the Craik-Leibovich equation follows then from the boundary problem

$$2w_2^E \partial_z w_2^E + \Xi\, e^{2z} \left[3\left(2w^S - w^s\right)\partial_z w_2^E + 2w^S\, \partial_r (r w_2^E)\right] = 0,$$
$$w_2^E(k,z) = -\Xi\, e^{2z}\, p_0, \quad |w_2^E(0,z)| < \infty. \quad (5.7)$$

Substitution $w_2^E(r,z) = \Xi e^{2z} w^E(r)$ reduces (5.7) to the boundary value problem for the Bernoulli differential equation

$$2\left(w^E\right)^2 + 3\left(2w^S - w^s\right) w^E + w^S \left(r w^E\right)' = 0, \ |w^E(0)| < \infty, \ \ w^E(k) = -p_0, \quad (5.8)$$

which has an exact analytical solution and causes

$$\boldsymbol{w}^E = \Xi e^{2z} w^E(r)\, \hat{\boldsymbol{\theta}}, \ \ w^E(r) = \frac{w^S(r)}{(c_0 r^2 - 1)}, \ c_0 = \frac{1}{k^2}\left(1 - \frac{w^S(k)}{p_0}\right), \quad (5.9)$$

where $w^S(r)$ is associated with the Stokes drift velocity (3.9); one should require $c_0 < k^{-2}$ to avoid singularity on the interval $0 \leqslant r \leqslant k$.

When $p_0 = p_0^s$, the resulting mean azimuthal mass-transport velocity reads as

$$\boldsymbol{w}^P = \boldsymbol{w}^s + \boldsymbol{w}^E = \Xi e^{2z} w^P(r) \hat{\boldsymbol{\theta}} = \Xi e^{2z} \left(\frac{J_1^2(r)}{r} + \frac{w^S(r)}{c_0 r^2 - 1}\right) \hat{\boldsymbol{\theta}}, \quad (5.10)$$

where $w^S$ comes from (3.9) and $c_0 = 0.10398523061\ldots$ .

The inviscid theoretical prediction (5.10) includes three consequent multipliers,

$$\Xi = O(\epsilon^{2/3}), \ \ e^{2z} \ (\text{where } |z| = O(1)) \ \text{ and } \ w^P(r) = O(1), \quad (5.11)$$

where $\Xi$ is responsible for the wave amplitude ($\Xi = ab$ for the undamped sloshing), $e^{2z}$ implies the exponential decay (the formula is true only for fairly deep liquid depths) and $w^P(r)$ describes the radial distribution of the mean mass-transport velocity. As remarked in § 2, the wave amplitude multiplier $\Xi$ can have a feedback from the mean mass-transport, i.e., the potential-flow values $a, \bar{a}, \bar{b}, b$ by Faltinsen *et al.* (2016) provide only an estimate of $\Xi$. Dependence of $a, \bar{a}, \bar{b}$ and $b$ on $\boldsymbol{w}^P$ goes beyond these studies. Finally, the exponential decay multiplier is formally of the order $O(1)$, which means that (5.10) is applicable only for $z$ far away from the mean free surface.

*Remark.* If we assume (even though we proved that it is not true), that the non-Eulerian mass-transport is described by $\boldsymbol{w}^S$, i.e. $\boldsymbol{w}^P = \boldsymbol{w}^L = \boldsymbol{w}^S + \boldsymbol{w}^E$, and, in addition, require the experimental peculiarity (b) implying $\boldsymbol{w}^E = -\boldsymbol{w}^S$ at $r = k$, the parameter $p_0$ in (5.9) becomes equal to $w(k)$ that gives $c_0 = 0 \Rightarrow w^E(r) = -w^S(r)$. The latter means that the return flow $\boldsymbol{w}^E$ fully annihilates $\boldsymbol{w}^S$ in each inner point of the liquid domain and, therefore, the total mass-transport becomes zero, at least, within the framework of the inviscid hydrodynamic model. This confirms that the first-order radial Lagrangian fluid particles displacements through the tank axis, which were extensively discussed in § 4 as causing the difference between $\boldsymbol{w}^s$ and $\boldsymbol{w}^S$, play an important role in the description of the Prandtl phenomenon.

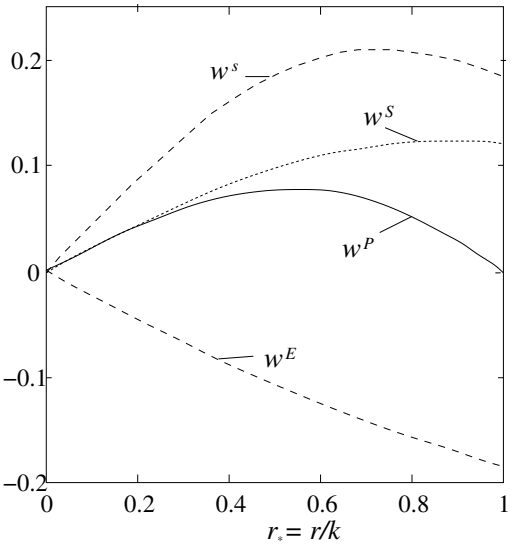


FIGURE 2. Functions $w^s(k\,r_*)$ by (4.7), $w^E(k\,r_*)$ by (5.9), and $w^P(k\,r_*)$ by (5.10), which represent the radial distribution of the mean non-Eulerian, Eulerian, and resulting mass-transport azimuthal velocities, respectively, by the $r_0$-scaled radial coordinate $r_* = r/k$. The graph $w^S(k\,r_*)$ illustrates the Stokes azimuthal mean velocity by (3.9).

## 6. Comparison with experiments

Figure 2 presents the theoretical azimuthal mass-transport velocity and its components along the $r_0$-scaled radial axis (the nondimensional radial coordinate $r_* = r/k$). These contain $w^s$ (the non-Eulerian mean, (4.7)), $w^E$ (the Eulerian mean, (5.9)) and $w^P$ (summarised mass-transport (5.10)). In addition, we depict the non-modified azimuthal Stokes drift velocity $w^S$, which is governed by (3.9) and appears in the Craik-Leibovich equation.

The non-Eulerian mean velocity is co-directed with the swirl-type propagating wave, $w^s(k\,r_*) > 0$, $0 < r_* < 1$ but the Eulerian-mean velocity counter-acts it, i.e., $w^E(k\,r_*) < 0$, $0 < r_* < 1$; here, $r_* = r/k$ is the $r_0$-scaled radial coordinate. This implies, in particular, that comparing the experimental data with, independently, $w^s$ and $w^E$ has no meaning. The sign of $w^E$ (the return flow) is opposite to the experimental discoveries, but $w^s$ does not satisfy, by itself, the experimental peculiarity (b) (zero azimuthal mass-transport on the vertical wall). Only the *summarised mass-transport* distribution $w^P$ (joint effect of $w^s$ and $w^E$) has a physical meaning for the studied problem and can be adopted for the forthcoming experimental validation. Obviously, $w^P$ satisfies the experimental peculiarities (a) and (b) (see, the Introduction).

The summarised mass-transport $w^P$ reaches its maximum value at about the semi-radius (satisfies the experimental peculiarity (c)) so that its graph has an arc-type shape. This shape is independent of the forcing frequency and amplitude (see, discussions on that by Bouvard *et al.* 2017; Reclari 2013; Hutton 1964).

Another interesting result is that $(w^P)'(0)$ is equal to $(w^S)'(0) = \frac{1}{8}$,

$$w^P(r) - w^S(r) = (-0.02862315382...)\,r^3 + O(r^5),$$

and, as a consequence, $\boldsymbol{w}^P$ is satisfactory fitted by the Stokes drift (3.9) in a neighbourhood of the tank centre (satisfies the experimental peculiarity (d)). The latter experimental fact was discussed by Bouvard *et al.* (2017) who commented that the mean

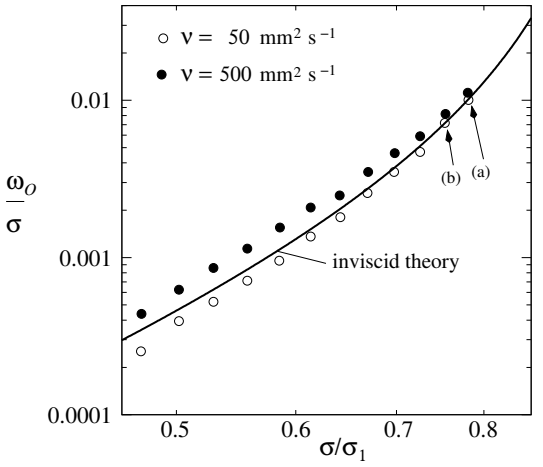


FIGURE 3. Theoretical prediction (6.1) of the nondimensional angular velocity $(\omega_O)_* = \omega_O/\sigma$ in the tank centre ($r_* = 0$ and $z_0^* = z_0/r_0 = -0.23$), the solid line, and the corresponding measured data by Bouvard *et al.* (2017) for two liquids with $\nu = 50\,\mathrm{mm}^2\,\mathrm{s}^{-1}$ (empty circles) and $\nu = 500\,\mathrm{mm}^2\,\mathrm{s}^{-1}$ (filled circles). The tank is exposed to the circular orbital forcing with the $r_0$-scaled amplitude $\eta_a^* = 0.057$. Experiments (a) and (b) were done with $\sigma/\sigma_1 = 0.78$ and 0.75, respectively. Theoretical amplitude parameter $\Xi$ is computed by using the linear sloshing theory with potential flows. The logarithmic scale is kept from the original publication by Bouvard *et al.* (2017).

mass-transport flow is nearly in solid-body rotation near the centre, rotating in the direction of the orbital shaking, for $0 < r_* < 0.3$. Comparing $w^P$ with $w^S$ in figure 2 confirms this interval of $r_*$.

In summary, the constructed solution satisfies all the experimentally-established peculiarities, which were listed in the Introduction, and, therefore, it *qualitatively* describes the Prandtl phenomenon. The next step consists of a *quantitative* validation of the analytical result (5.10). Limitations of the Narimanov-Moiseev theory (i)-(iv) (see, § 2) and a lack of measurements of the Prandtl mass-transport phenomenon (including his pioneering work) for fairly deep liquid depths makes it difficult to find suitable experimental data for this validation. With known reservations, only measurements by Hutton (1964) and Bouvard *et al.* (2017) can be adopted.

### 6.1. *Experiments by Bouvard* et al. *(2017)*

By using a very special *stroboscopic* PIV velocimetry technique, which makes it possible to detect the mass transport, Bouvard *et al.* (2017) measured the azimuthal mass-transport (corresponds to $\boldsymbol{w}^P$) and mean radial (associated with $w_1^E = 0$ in our inviscid theory) velocities for swirling waves occurring due to the orbital horizontal circular forcing of the tank. In these experiments, the upright circular container was filled, consequently, by two different silicon oils so that the experimental series were characterised by Reynolds numbers equal to $Re_s = r_0^2\sigma/(k^2\nu) = 1000/k^2$ ($\nu = 50$ mm$^2$ s$^{-1}$) and $100/k^2$ ($\nu = 500$ mm$^2$ s$^{-1}$), respectively ($\nu$ is the kinematic viscosity). Silicon oil with with $\nu = 500$ mm$^2$ s$^{-1}$ is definitely *not* low-viscous. The measurements were done at the horizontal level $z_0^* = z_0/r_0 = -0.23$, which is relatively far from the free surface, $|z_0| = 0.23\,k = O(1)$ and, therefore, formula (5.10) is applicable.

The liquid depth was sufficiently large, $h_* = h/r_0 = 2.168$, ($r_0 = 51.2$ mm, the Bond number is about 500 so that surface tension can be neglected). The forcing amplitude

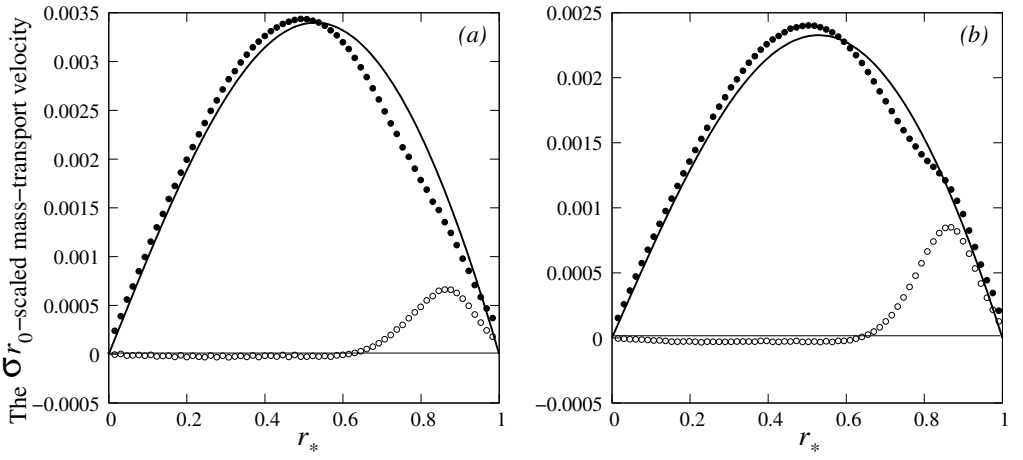


FIGURE 4. The $r_0\sigma$-scaled measured (Moisy, personal communication) and theoretical (6.2) liquid mass-transport velocity in the azimuthal (solid circles and solid arc-type line, respectively) and radial (empty circles, the theory states zero) directions. The results with $z_0^* = -0.23$, the forcing frequencies $\sigma/\sigma_1 = 0.78$ (a) and 0.75 (b), the forcing amplitude $\eta_1^* = 0.057$ (circular tank motions). The experimental tank has the nondimensional depth $h_* = h/r_0 = 2.168$.

was $O(\epsilon) = \eta_a^* = \eta_{1a}/r_0 = \eta_{2a}/r_0 = 0.057$, but the tested forcing frequencies were in the range $0.48 \lesssim \sigma/\sigma_1 \lesssim 0.78$, which is generally speaking, away from the primary resonance zone, $0.9 \lesssim \sigma/\sigma_1 \lesssim 1.07$, where the Moiseev detuning condition (2.6) is fulfilled. Finally, the experimental frequency range contains rather dangerous secondary resonances by the first axisymmetric (01) mode at $\sigma/\sigma_1 = 0.72$ (see, an extra small amplitude-response peak about this value in experiments by Reclari 2013) and for the asymmetric (21) mode ($\sigma/\sigma_1 = 0.65$).

Summarising the aforementioned input parameters shows that conditions (i), (iii), and (iv) (see, § 1) are, generally, not satisfied. However, the approximate analytical result (5.10) can, for experiments by Bouvard *et al.* (2017), be interpreted as the *single* $J_1$-*mode* approximation on the azimuthal mass-transport within the framework of the *linear* sloshing theory.

Our first focus is on the mean angular liquid velocity $\omega_O$ in the tank centre, which can, according to (5.10), be estimated as $\omega_O/\sigma = \Xi e^{kz_0^*}(w^P)'(0) = \frac{1}{8}\Xi e^{kz_0^*}$, $z_0^* = z_0/r_0$, where $z_0$ is the dimensional horizontal level beneath the mean free surface. Adopting the single-mode linear potential-flow sloshing prediction of the amplitude parameter $\Xi$ (Faltinsen & Timokha 2009, Chapter 5) derives the formula

$$\frac{\omega_O}{\sigma} = \frac{1}{8}(k^2\eta_a^*\alpha)^2 e^{2kz_0^*}\left(\left(\frac{\sigma_1}{\sigma}\right)^2 - 1\right)^{-2}, \quad \alpha = \frac{\int_0^k r^2 J_1(r)\mathrm{d}r}{\int_0^k r J_1^2(r)\mathrm{d}r}, \tag{6.1}$$

which is compared with the measured data by Bouvard *et al.* (2017) in figure 3 (the measured values for $\nu = 50\,\mathrm{mm}^2\,\mathrm{s}^{-1}$ are marked by the empty circles but $\nu = 500\,\mathrm{mm}^2\,\mathrm{s}^{-1}$ corresponds to the filled circles). The logarithmic axis scale is kept from the original experimental work.

Figure 3 demonstrates that viscosity matters for $\nu = 500\,\mathrm{mm}^2\,\mathrm{s}^{-1}$ so that the theory only qualitatively fits the corresponding measured values. As for silicon oil with $\nu = 50\,\mathrm{mm}^2\,\mathrm{s}^{-1}$, discrepancy for $\sigma/\sigma_1 < 0.75$ is theoretically clarified by the aforementioned secondary resonances at $\sigma/\sigma_1 = 0.72$ and 0.65, but the theory shows a good agreement

for the cases (a) ($\sigma/\sigma = 0.78$) and (b) ($\sigma/\sigma = 0.75$), which are away from the secondary resonances but close to the primary resonance zone. The latter closeness means an increasing contribution of the lowest natural sloshing mode.

When preparing the paper, Bouvard *et al.* (2017) measured azimuthal and radial components of the mean mass-transport as function of $r_*$ ($z_0^* = -0.23$). Professor F. Moisy (personal communication) granted us with these $r_0\sigma$-scaled measured data. Adopting, as in (6.1), the linear potential-flow sloshing theory for computing the amplitude parameter $\Xi$ derives the formula

$$(w_1^P)_* = (w_3^P)_* = 0, \quad (w_2^P)_* = k(\eta_a^*\alpha)^2 e^{2kz_0^*}\left(\left(\frac{\sigma_1}{\sigma}\right)^2 - 1\right)^{-2} w^P(k\, r_*) \tag{6.2}$$

from (5.10).

Figure 4 compares (6.2) with the measured data by Moisy (personal communication) for the cases (a) and (b) in figure 3. Specifically, (6.2) states that the radial mean mass-transport is zero ($(w_1^P)_* \equiv 0$) because we neglect the poloidal recirculation and other viscous non-azimuthal mean streams. Figure 4 supports the neglecting – the measured radial mean mass-transport is zero for $0 < r_* < 0.7$ but, even though this mass-transport is not zero on the interval $0.7 < r_* < 1$, it is clearly lower than the measured azimuthal mass-transport. This is especially for the case (a), whose forcing frequency is relatively close to the Narimanov-Moiseev resonant zone.

As for the azimuthal mass-transport velocity in figure 4 (solid arc and filled circles), the constructed inviscid theory by (6.2) demonstrates *quantitatively good* prediction. Especially, if we recall that the theory neglects viscous flows and adopts the approximate single-mode linear sloshing solution for computing the amplitude parameter $\Xi$.

### 6.2. *Experiments by Hutton (1964)*

Another experimental series for swirling wave mode was reported by Hutton (1964). He used the longitudinal harmonic excitation ($\eta_{1a} \neq 0$, $\eta_{2a} = 0$) with the forcing frequency equal to $\sigma = \sigma_1$, i.e., when the swirling wave mode is stable and possesses the same features as for the orbital forcing (Faltinsen *et al.* 2016). Hutton (1964) utilised three different forcing amplitudes, which were, unfortunately, *not* specified in the original paper but, instead, he distinguished the corresponding experimental series by documenting the experimental crest ($e_{\max}$) and through ($e_{\min}$) at the wall in the excitation plane (see, figure 5). The geometric input was $r_0 = 22.47$ cm, $h = 31.45$ cm ($h_* = h/r_0 = 1.4$), $\sigma_1 = 8.91$ rad s$^{-1}$. Tap water with $\nu = 10^{-6}$ m$^2$/s and $Re_s = 4.5 \cdot 10^5$.

To measure the azimuthal mass-transport velocity distribution, Hutton (1964) used a mechanical device ('fixture') whose main element is a rectangular paddle lying in the meridional plane and rotating together with the contained liquid as depicted in figure 5. Three different paddles were employed, which are denoted as 'small paddle' (rectangle sides are $l_r \times l_z$=3.937×2.286 cm), 'medium paddle' (4.8514×3.6068 cm) and 'large paddle' (5.968×4.334 cm). The measurements were made at the vertical levels $z_0^* = -0.59\,(z_0^* = -0.43\,h)$, $z_0^* = -0.92\,(z_0^* = -0.67\,h)$, and $z_0^* = -1.22\,(z_0^* = -0.89\,h)$. Hutton (1964) wrote that *"the test data also indicated that the transport velocity was nearly constant over the range of depths"*, which means that the azimuthal mass-transport velocity does not depend on $z$ (as in (5.10)) due to the bottom effect for the liquid filling $h_* = h/r_0 = 1.4$, which is not fairy deep. The experimental input in Hutton (1964) satisfies condition (i), (iii) and (iv) in § 2 but does not (ii).

The azimuthal mass-transport velocities were normalised by its maximum value and compared with our inviscid analytical solution (5.10), $w^P(r)/\max|w^P|$. The result is presented in figure 5. The smaller symbol implies the smaller paddle. The filling depth

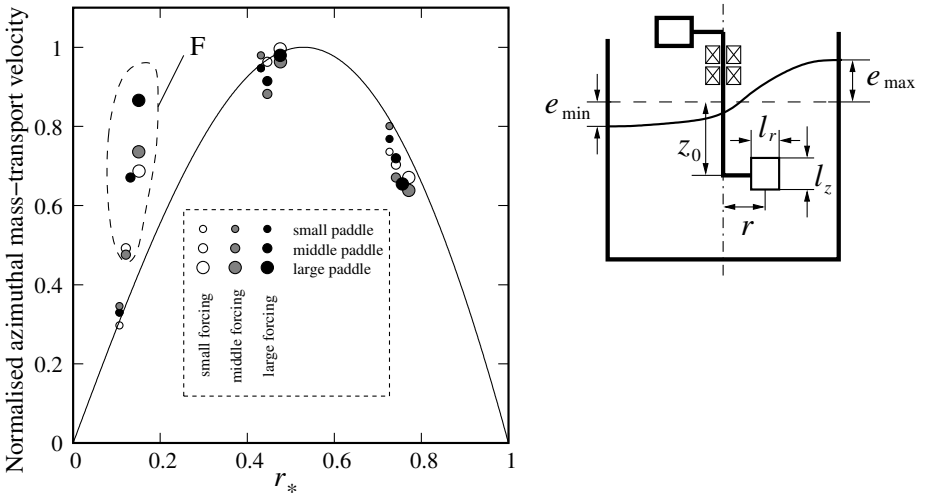


FIGURE 5. The azimuthal mass-transport velocity scaled by its maximum value for the experimental case by Hutton (1964), which were done with tap water ($Re_s = 4.5 \cdot 10^5$), $r_0 = 22.46884$ cm, $h_* h/r_0 = 1.4$. Swirling wave mode was excited by the horizontal longitudinal tank forcing along the $Ox$ axis ($\eta_{2a} = 0$) with the forcing frequency $\sigma = \sigma_1$, for which, according to Faltinsen *et al.* (2016), the swirling wave mode is stable. The measurements were dome at the vertical level $z_0 = -0.43\, h$, $z_0^* = -0.59$. Three different forcing amplitudes (denoted as small, middle and large) were used, which are not specified by Hutton (1964) who has linked these three experimental cases to experimental crest ($e_{\max}$)/trough ($e_{\min}$) at the wall equal to 8.89/5.334, 11.43/6.35, and 13.97/7.62 cm, respectively. The experimental setup employed a mechanical measurement technique with rectangular paddles of different sizes. The sizes are marked as 'small paddle' = $l_r \times l_z$=3.937×2.286 cm; 'medium paddle' = 4.8514×3.6068 cm; 'large paddle' = 5.968×4.334 cm. The measurements in zone F can according to Hutton (1964) be affected by the paddle feedback on the liquid flows.

of the used symbols also increases with increasing the forcing amplitude (Hutton 1964, reports the experimental crest ($e_{\max}$)/trough ($e_{\min}$) of azimuthal progressive wave at the wall for these three forcing amplitudes as 8.89/5.588, 11.43/6.35, and 13.97/7.62 cm, respectively). Figure 5 supports our analytical inviscid solution for measurements made with 'small paddle'. 'Medium' and 'large' paddles give clearly larger values for one measurement probe, which is closely located to the tank centre. Hutton (1964) suggested that bigger paddles may yield a feedback on the liquid flows for the latter case.

As we mentioned above, because the liquid depth $h_*$ was not large enough and the nearly-bottom flows matter, Hutton (1964) states that there is no exponential decay $e^{2z}$ as predicted in (5.10). Hutton (1964) reports that the azimuthal mass-transport is uniquely function of $r$. Speculatively assuming that the nearly-bottom flows play an 'averaging role', one can take the mean value of $e^{2z}$ over the infinite depth, which implies replacement $e^{2z} \to \int_{-\infty}^{0} e^{2z} \mathrm{d}z = \frac{1}{2}$. Furthermore, one can roughly approximate the amplitude parameters

$$a = \frac{k\,(e_{\max} + e_{\min})}{2\, r_0\, J_1(k)} + O(\epsilon), \quad b = a\sqrt{\frac{m_3}{m_1}} = a\sqrt{1.83...}$$

(meaning of coefficients $m_1$ and $m_3$ is explained by Faltinsen *et al.* 2016) and formula

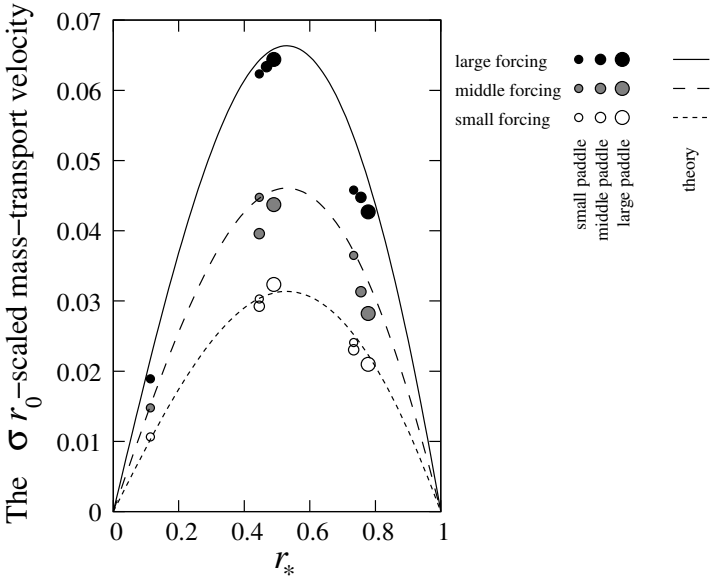


FIGURE 6. Comparison of theoretical formula (6.3) with measured data by Hutton (1964) with the input parameters documented in the caption of figure 5. Measurements from zone Z, where the azimuthal mass-transport was measured with relatively large paddles, which influence the liquid flows, were excluded.

(5.10) transforms then to the approximate form

$$(w_2^P)_* = \frac{k\sqrt{1.83}}{2J_1^2(k)} e_*^2 w^P(k\, r_*), \quad e_* = \frac{e_{\max} + e_{\min}}{2r_0} \tag{6.3}$$

for the $r_0\sigma$-scaled azimuthal mass-transport velocity.

The theoretical prediction (6.3) is compared with the measured data by Hutton (1964) except from zone F in figure 5, where, as we stated, the larger paddle feedbacks the liquid flows. The theoretical results by (6.3) look sufficiently good if we account for how many assumptions were made to derive formula (6.3).

## 7. Conclusions

The mean azimuthal liquid mass-transport (Prandtl' phenomenon, 1949) generated by swirling waves in a vertical circular cylindrical tank with an infinite liquid depth is theoretically described by using the asymptotic steady-state wave solution (potential flows of incompressible liquid) by Faltinsen *et al.* (2016). The summarised mass-transport velocity is associated with $\boldsymbol{w}^P = \boldsymbol{w}^E + \boldsymbol{w}^s$, where $\boldsymbol{w}^E$ is the Eulerian-mean (vortical) velocity, which appears as a second-order supplement to the asymptotic inviscid solution by Faltinsen *et al.* (2016) and $\boldsymbol{w}^s$ is the non-Eulerian mean, which is affected by the Stokes drift and the first-order radial inflow/outflow into the meridional plane at $r = 0$. The non-Eulerian mass-transport component $\boldsymbol{w}^s$ is co-directed with azimuthally-propagating (swirling) wave, but $\boldsymbol{w}^E$ implies the return flow.

The Eulerian-mean velocity $\boldsymbol{w}^E$ is governed by the inviscid Craik-Leibovich equation whose special analytical form is derived in the present paper by using the time-averaging in the vorticity equation. Finding a unique $\boldsymbol{w}^E$ requires to know tangential

boundary conditions on the wall. Derivations of these conditions from the nonlinear Eulerian boundary-layer analysis (see, the Supplementary Materials B) does not fit the existing experimental peculiarities of the summarised azimuthal mass-transport, and causes mathematical conflict with the used asymptotic scheme in a neighbourhood of the contact curve between the liquid surface and the tank wall. The failure is, in our opinion, caused by the neglecting of the fluid particles motion by $\boldsymbol{w}^s$ in a neighbourhood of the wall, which acts on viscous stresses and yields an extra vorticity. In the *inviscid* limit, we suggest that local mass-transport $\boldsymbol{w}^s$ at the wall implies dominant mechanism to constitute the Eulerian-mean flow. Physically, this implies that typical viscous vortical streams are neglected. Mathematically, this means that one can use the inviscid Craik-Leibovich boundary problem, but adopt the time-averaged no-slip condition for the resulting (Eulerian + non-Eulerian) particle velocities on the wall. The latter causes the tangential boundary condition $\boldsymbol{w}^E = -\boldsymbol{w}^s$ on the wall. This tangential condition can be treated as an analogy of the Kutta-Joukowski condition for steady ambient flow past a stationary foil but for the studied problem. Provided by this tangential boundary condition, we were able to derive $\boldsymbol{w}^P$ in a simple analytical form. The theoretical result is compared with the measured data by Bouvard *et al.* (2017) and Hutton (1964). The results are in a good quantitative agreement. The comparison confirms that viscosity and associated viscous streams may play a secondary role for the mass-transport phenomenon by Prandtl.

The present paper neglects a feedback of the mean liquid rotation on the lowest-order amplitudes $a, b, \bar{a}$ and $\bar{b}$, which are taken from the steady-state asymptotic solution by Faltinsen *et al.* (2016). This fact as well as the nearly-bottom flow effect deserve dedicated studies.

The authors acknowledge the financial support of the Centre of Autonomous Marine Operations and Systems (AMOS) whose main sponsor is the Norwegian Research Council (Project number 223254–AMOS). The authors also thank Professor F. Moisy for providing unpublished experimental data, which are used for comparative analysis in figure 4.

## REFERENCES

Batchelor, G. K. 2000 *An introduction to fluid dynamics*. Cambridge University Press.

Bouvard, J., Herreman, W. & Moisy, F. 2017 Mean mass transport in an orbitally shaken cylindrical container. *Physical Review Fluids* **2**, Paper No 084801.

Bremer, T. S. van den & Breivik, Ø. 2017 Stokes drift. *Philosophical Transactions A: Mathematical, Physical and Engineering Sciences* **376** (2111), A 2018 376 20170104.

Bühler, O. 2009 *Waves and mean flows*. Cambride University Press.

Craik, A. D. 1986 *Wave interaction and fluid flows*. Cambridge University Press.

Craik, A. D. & Leibovich, S. 1976 A rational model for Langmuir circulations. *Journal of Fluid Mechanics* **73** (3), 401–426.

Ducci, A. & Weheliye, W. H. 2014 Orbitally shaken bioreactors-viscosity effects on flow characteristics. *AIChE Journal* **60** (11), 3951–3968.

Faltinsen, O. M., Lukovsky, I. A. & Timokha, A. N. 2016 Resonant sloshing in an upright annular tank. *Journal of Fluid Mechanics* **804**, 608–645.

Faltinsen, O. M. & Timokha, A. N. 2009 *Sloshing*. Cambridge: Cambridge University Press.

Hutton, R. E. 1964 Fluid-particle motion during rotary sloshing. *Journal of Applied Mechanics, Transactions ASME* **31** (1), 145–153.

Kochin, N. E., Kibel, I. A. & Roze, N. V. 1965 *Theoretical hydromechanics*. New York, London, Sydney: John Wiley & Sons, Ltd.

Leibovich, S. 1980 On wave-current interaction theories of Langmuir circulations. *Journal of Fluid Mechanics* **99** (4), 715–724.

Moiseev, N. N. 1958 On the theory of nonlinear vibrations of a liquid of finite volume. *Journal of Applied Mathematics and Mechanics* **22** (5), 860–872.

Polyanin, A. D. & Nasaikinskii, V. E. 2015 *Handbook of linear partial differential equations for engineers and scientists (second edition)*. CRC Press, Taylor & Francis Group.

Prandtl, L. 1949 Erzeugung von Zirkulation beim Schütteln von Gefässen. *ZAMM* **29** (1/2), 8–9.

Reclari, M. 2013 Hydrodynamics of orbital shaken bioreactors. Thesis no 5759 (2013), Ècole Polytechnique Federale de Lausanne.

Reclari, M., Dreyer, M., Tissot, S., Obreschkow, D., Wurm, F. M. & Farhat, M. 2014 Surface wave dynamics in orbital shaken cylindrical containers. *Physics of Fluids* **26**, Paper ID 052104.

Riley, N. 2001 Steady streaming. *Annular Review of Fluid Mechanics* **33**, 43–65.

Royon-Lebeaud, A., Hopfinger, E.J. & Cartellier, A. 2007 Liquid sloshing and wave breaking in circular and square-base cylindrical containers. *Journal of Fluid Mechanics* **577**, 467–494.

## SUPPLEMENTARY MATERIALS

## Appendix A. Explicit form of the Craik-Leibovich equation

Explicit form of the continuity equation (3.2) in cylindrical coordinate system can be written as

$$\partial\Omega_1^E + \partial\Omega_3^E = -\frac{1}{r}\left(\Omega_1^E + \partial\Omega_1^E\right). \tag{A 1}$$

Using (A 1) and definition of the Stokes drift (3.9) utilise the derivation line

$$\begin{aligned}\nabla\times\left[\boldsymbol{w}^S\times\boldsymbol{\Omega}^E\right] = \nabla\times\left[\hat{\boldsymbol{r}}\left(w\Omega_2^E\right) - \hat{\boldsymbol{z}}\left(w\Omega_1^E\right)\right] = -\frac{1}{r}w\left[\hat{\boldsymbol{r}}\partial_\theta\Omega_1^E + \hat{\boldsymbol{z}}\partial_\theta\Omega_3^E\right]\\ + \hat{\boldsymbol{\theta}}\left[\partial_z\left(w\Omega_3^E\right) + \partial_r\left(w\Omega_1^E\right)\right] = -\Xi e^{2z}\frac{1}{r}w^S\left[\hat{\boldsymbol{r}}\partial_\theta\Omega_1^E + \hat{\boldsymbol{z}}\partial_\theta\Omega_3^E\right]\\ + \hat{\boldsymbol{\theta}}\left[2w\Omega_3^E + w\left(\partial_z\Omega_3^E + \partial_r\Omega_1^E\right) + \Omega_1^E\partial_r w\right]\\ = -\Xi e^{2z}\left(\frac{1}{r}w^S\,\partial_\theta\boldsymbol{\Omega}^E - \hat{\boldsymbol{\theta}}\left[\left((w^S)' - \frac{1}{r}w^S\right)\Omega_1^E + 2w^S\,\Omega_3^E\right]\right).\end{aligned}$$

Adopting the Bessel function definition $J_1'' = -r^{-1}J_1' - J_1 + r^{-2}J_1$ and employing the Maplesoft analytical manipulator derive

$$(w^S)' - \frac{1}{r}w^S = -\frac{3}{r}\left[\frac{1}{r}\left(J_1' - \frac{J_1}{r}\right)^2\right] = -\frac{3}{r}\left[2w^S - w^s\right].$$

## Appendix B. Nonlinear (Eulerian-mean) boundary-layer effect

The boundary layer analysis starts with adopting, as in the main paper body, the characteristic length $r_0/k$ and time $1/\sigma$. This mathematically computes the corresponding Reynolds number $Re_s = (r_0^2\sigma)/(\nu k) \gg 1$, where $\nu$ is the kinematic viscosity. Transition and turbulent flow is neglected that implies an upper bound for applicable Reynolds numbers (Eq. (6.2.3) in Faltinsen & Timokha 2009).

### B.1. *Nonlinear boundary-layer equations*

We consider, in parallel way, the non-dimensional inviscid ambient velocity field $\boldsymbol{v}(r,\theta,z,t) = v_1\hat{\boldsymbol{r}} + v_2\hat{\boldsymbol{\theta}} + v_3\hat{\boldsymbol{z}}$ containing the non-zero mean-flow component $\boldsymbol{w}^E(r,\theta,z) = \langle\boldsymbol{v}\rangle = w_1^E\hat{\boldsymbol{r}} + w_2^E\hat{\boldsymbol{\theta}} + w_3^E\hat{\boldsymbol{z}}$, which is associated with (generally, unknown *a priori*) steady streaming, and the non-dimensional velocity field $\boldsymbol{V}(r,\theta,z,t) = U\hat{\boldsymbol{r}} + V\hat{\boldsymbol{\theta}} + W\hat{\boldsymbol{z}}$, which is affected by the viscous boundary layer at the vertical wall. We need also the ambient pressure field $p$ and $P$, which is associated with the viscous velocity field, forgetting on the first stage that these are the same in the lowest-order approximation (this fact will be shown later, mathematically).

The viscous flow is governed by the continuity equation

$$(rU)_r + V_\theta + r\,W_z = 0, \tag{B 1}$$

and the nondimensional Navier–Stokes equation

$$\begin{aligned}\dot{U} + UU_r + \frac{VU_\theta}{r} - \frac{V^2}{r} + WU_z = -P_r + \delta^2\left[\frac{(rU_r)_r}{r} - \frac{U}{r^2} + \frac{U_{\theta\theta}}{r^2} - \frac{2V_\theta}{r^2} + U_{zz}\right]\\ + \cos\theta\ddot{\eta}_1 + \sin\theta\ddot{\eta}_2,\end{aligned} \tag{B 2a}$$

$$\dot{V}+UV_r+\frac{VV_\theta}{r}+\frac{UV}{r}+WV_z=-\frac{P_\theta}{r}+\delta^2\left[\frac{(rV_r)_r}{r}-\frac{V}{r^2}+\frac{V_{\theta\theta}}{r^2}+\frac{2U_\theta}{r^2}+V_{zz}\right] - \sin\theta\ddot{\eta}_1+\cos\theta\ddot{\eta}_2, \quad (\mathrm{B}\,2b)$$

$$\dot{W}+UW_r+\frac{VW_\theta}{r}+WW_z=-P_z+\delta^2\left[\frac{r(W_r)_r}{r}+\frac{W_{\theta\theta}}{r^2}+W_{zz}\right], \quad (\mathrm{B}\,2c)$$

where $\delta=\sqrt{1/Re_s}$ is an asymptotic measure of the boundary layer thickness $\delta$ at the vertical wall and, therefore, $\delta$ is small parameter, which is assumed be smaller than the forcing amplitude (2.5).

The viscous-flow velocity field must satisfy the *no-slip condition* at the wall and tend to the inviscid velocity field (*including* the steady streaming component $\boldsymbol{w}^E$) away from the boundary layer. These two conditions can mathematically be formalised as

$$\boldsymbol{V}=\boldsymbol{0} \ \text{ at } \ r=k \quad \text{and} \quad ||\boldsymbol{V}-\boldsymbol{v}||=O(\delta) \ \text{ as } \ k-r\gg O(\delta). \quad (\mathrm{B}\,3)$$

The forthcoming asymptotic derivations will be done in terms of the *differences*

$$\boldsymbol{\mathcal{V}}=\boldsymbol{V}-\boldsymbol{v}=(R,\Theta,Z)=(U-u,V-v,W-w) \text{ and } \ \mathcal{P}=P-p, \quad (\mathrm{B}\,4)$$

between viscous and ambient flow parameters.

Because the ambient flow satisfies (B 1), (B 2) *with* $\delta=0$, the governing equations for the differences take the form

$$(rR)_r+\Theta_\theta+r\,Z_z=0, \quad (\mathrm{B}\,5a)$$

$$\dot{R}+RR_r+\frac{\Theta R_\theta}{r}-\frac{\Theta^2}{r}+ZR_z+[uR_r+Ru_r]+\frac{1}{r}[vR_\theta+\Theta u_\theta]-\frac{2\Theta v}{r}+[Zu_z+wR_z]=-\mathcal{P}_r + \delta^2\left[\frac{(rR_r)_r}{r}-\frac{R}{r^2}+\frac{R_{\theta\theta}}{r^2}-\frac{2\Theta_\theta}{r^2}+R_{zz}\right]+\delta^2\left[\frac{(ru_r)_r}{r}-\frac{u}{r^2}+\frac{u_{\theta\theta}}{r^2}-\frac{2v_\theta}{r^2}+w_{zz}\right], \quad (\mathrm{B}\,5b)$$

$$\dot{\Theta}+R\Theta_r+\frac{\Theta\Theta_\theta}{r}+\frac{R\Theta}{r}+Z\Theta_z+[u\Theta_r+Rv_r]+\frac{1}{r}[v\Theta_\theta+\Theta v_\theta]+\frac{1}{r}[u\Theta+Rv]+[w\Theta_z+Zv_z]= -\frac{\mathcal{P}_\theta}{r}+\delta^2\left[\frac{(r\Theta_r)_r}{r}-\frac{\Theta}{r^2}+\frac{\Theta_{\theta\theta}}{r^2}+\frac{2R_\theta}{r^2}+\Theta_{zz}\right]+\delta^2\left[\frac{(rv_r)_r}{r}-\frac{v}{r^2}+\frac{v_{\theta\theta}}{r^2}+\frac{2u_\theta}{r^2}+v_{zz}\right], \quad (\mathrm{B}\,5c)$$

$$\dot{Z}+RZ_r+\frac{\Theta Z_\theta}{r}+ZZ_z+[uZ_r+Rw_r]+\frac{1}{r}[vZ_\theta+\Theta w_\theta]+[wZ_z+Zw_z] = -\mathcal{P}_z+\delta^2\left[\frac{r(Z_r)_r}{r}+\frac{Z_{\theta\theta}}{r^2}+Z_{zz}\right]+\delta^2\left[\frac{r(w_r)_r}{r}+\frac{w_{\theta\theta}}{r^2}+w_{zz}\right]. \quad (\mathrm{B}\,5d)$$

The no-slip condition (B 3) transforms to

$$\boldsymbol{\mathcal{V}}=(R,\Theta,Z)=\boldsymbol{V}-\boldsymbol{v}=(-v,-u,-w) \ \text{ at } \ r=k, \quad (\mathrm{B}\,6)$$

but the closeness of $\boldsymbol{V}$ and $\boldsymbol{v}$ far from the boundary layer will be rewritten as

$$||\boldsymbol{\mathcal{V}}||=O(\delta) \ \text{ for } \ (k-r)\gg O(\delta); \ \ 0\leqslant r<k. \quad (\mathrm{B}\,7)$$

To clarify what is the mathematical infinity for the closed domain, we introduce the

boundary-layer spatial variable $\xi$ as

$$r = k - \delta\xi, \quad 0 < \xi = O(1) \tag{B 8}$$

and consider the differences as functions of $\xi, t$ and $\theta, z$, i.e., $R = R(\xi, t; \theta, z), \Theta = \Theta(\xi, t; \theta, z), Z = Z(\xi, t; \theta, z)$ and $\mathcal{P} = \mathcal{P}(\xi, t; \theta, z)$. Furthermore, we look for the asymptotic solution of (B 5)-(B 7)

$$R = \delta R_1 + ..., \ \Theta = \Theta_0 + \delta\Theta_1 + ..., \ Z = Z_0 + \delta Z_1 + ..., \ \mathcal{P} = \delta\mathcal{P}_1 + ... . \tag{B 9}$$

One must note that $R_0 = 0$ because the normal velocity is zero at $r = k$, but the zero-order pressure difference $\mathcal{P}_0 = 0$ (the ambient pressure is continuous through the boundary layer) is according to (B 5$b$) rewritten in the $\xi, t$; $\theta, z$ coordinates.

Utilising the rule $(\cdot)_\xi = -\delta(\cdot)_r$ for $R$, $\Theta$ and $Z$ and keeping only the $O(1)$ terms derive

$$R_{1\xi} = Z_{0z} + \Theta_{0\theta}/k \tag{B 10}$$

from (B 5$a$), but (B 5$c$) and (B 5$d$) transform to the two equations

$$\dot{\Theta}_0 - \Theta_{0\xi\xi} - R_1\Theta_{0\xi} + \frac{\Theta_0\Theta_{0\theta}}{k} + Z_0\Theta_{0z} + \xi\bar{u}_r\Theta_{0\xi} + \frac{1}{k}[\bar{v}\Theta_{0\theta} + \bar{v}_\theta\Theta_0] + [\bar{w}\Theta_{0z} + \bar{v}_z Z_0] = 0, \tag{B 11$a$}$$

$$\dot{Z}_0 - Z_{0\xi\xi} - R_1 Z_{0\xi} + \frac{\Theta_0 Z_{0\theta}}{k} + Z_0 Z_{0z} + \xi\bar{u}_r Z_{0\xi} + \frac{1}{k}[\bar{v}Z_{0\theta} + \bar{w}_\theta\Theta_0] + [\bar{w}Z_{0z} + \bar{w}_z Z_0] = 0, \tag{B 11$b$}$$

in which the bars denote projections of the vector-function $\boldsymbol{v}$, and its derivatives, on the wall (these are simply expanded in a Taylor series by $\delta$) so that all coefficients in (B 11) become the known time-depending functions, which parametrically depend on $\theta$ and $z$,

$$\bar{u}_r(t;\theta,z) = u_r(k,\theta,z,t), \ \bar{v}(t;\theta,z) = v(k,\theta,z,t), \ \bar{v}_\theta(t;\theta,z) = v_\theta(k,\theta,z,t),$$
$$\bar{w}(t;\theta,z) = w(k,\theta,z,t), \ \bar{v}_z(t;\theta,z) = w_z(k,\theta,z,t).$$

Eqs. (B 4), (B 5) are, in fact, nonlinear boundary-layer equations, which are written in terms of the *differences* between viscous and inviscid (including steady streaming) components. According to (B 6), the solution of these 'difference field' equations (B 11) satisfies the *inhomogeneous* boundary conditions

$$R_1 = 0, \quad \Theta_0 = -\bar{v}, \quad Z_0 = -\bar{w} \ \text{ at } \ \xi = 0 \tag{B 12}$$

where the right-hand side is the minus projection of tangential components of the inviscid ambient flow.

Because $\Theta_0$, $Z_0 = O(1)$, but $R_1$ corresponds to the first-order approximation in (B 9), the asymptotic condition (B 7) transforms to the form

$$|\Theta_0| + |Z_0| \to 0 \text{ and } |R_1| \to O(1) \text{ as } \ \xi \to +\infty. \tag{B 13}$$

### B.2. *Asymptotic solution of the nonlinear boundary-layer problem*

The steady-state wave solution by Faltinsen *et al.* (2016) implies an asymptotic representation of the inviscid (ambient) velocity field by the small parameter $O(\epsilon^{1/3})$ where the lowest-order component takes the form (2.3) but the second-order approximation includes the steady-streaming component and is defined by (3.3). Because the nonlinear boundary-layer problem (B 10)–(B 13) governs the $O(1)$ approximation on the $O(\delta)$ scale and the asymptotic condition (2.5) is satisfied, one can consider an asymptotic approximation in

terms of $O(\epsilon^{1/3})$ as follows

$$\begin{aligned}&\Theta_0 = \Theta_0^{(1/3)} + \Theta_0^{(2/3)} + O(\epsilon)..., \quad Z_0 = Z_0^{(1/3)} + Z_0^{(2/3)} + O(\epsilon)...,\\ &R_1 = R_1^{(1/3)} + R_1^{(2/3)} + O(\epsilon)...\end{aligned} \tag{B 14}$$

for $\xi > 0$, $-\infty < t < \infty$ and $z < 0$, $-\pi \leqslant \theta < \pi$.

B.2.1. *The $O(\epsilon^{1/3})$ component*

Taking (2.3) derives that the first-order approximation of (B 10)–(B 12) comes from the *linear* parabolic problems ($\xi > 0$, $-\infty < t < \infty$):

$$\dot\Theta_0^{(1/3)} - \Theta_{0\xi\xi}^{(1/3)} = 0,\ \Theta_0^{(1/3)}(0,t;\theta,z) = -\frac{J_1(k)}{k} e^z \left[\cos t\, \theta_c'(\theta) + \sin t\, \theta_s'(\theta)\right], \tag{B 15a}$$

$$\dot Z_0^{(1/3)} - Z_{0\xi\xi}^{(1/3)} = 0,\ \ Z_0^{(1/3)}(0,t;\theta,z) = -J_1(k)\, e^z \left[\cos t\, \theta_c(\theta) + \sin t\, \theta_s(\theta)\right], \tag{B 15b}$$

which consists of the two independent linear Stokes boundary-layer equations (Batchelor 2000) parametrically dependent on $z < 0$, $-\pi \leqslant \theta < \pi$. The exact time-periodic solution of (B 15) reads, according to § 3.1.1 in Polyanin & Nasaikinskii (2015), as

$$\Theta_0^{(1/3)}(\xi,t;\theta,z) = -\frac{J_1(k)}{k}\, e^{z-\alpha\xi} \left[\theta_c'(\theta)\cos(t-\alpha\xi) + \theta_s'(\theta)\sin(t-\alpha\xi)\right], \tag{B 16a}$$

$$Z_0^{(1/3)}(\xi,t;\theta,z) = -J_1(k)\, e^{z-\alpha\xi} \left[\theta_c(\theta)\cos(t-\alpha\xi) + \theta_s(\theta)\sin(t-\alpha\xi)\right], \tag{B 16b}$$

($\alpha = 1/\sqrt{2}$), where the $e^{-\alpha\xi}$-multiplier corresponds to $e^{-\alpha(k-r)/\delta}$ in the original nondimensional $(r,\theta,z)$-coordinates, which exponentially decays and becomes small as $(k-r) = O(1)$.

Substituting (B 16) into the continuity equation (B 10) and using the first boundary condition of (B 12) gives

$$\begin{aligned}R_1^{(1/3)}(\xi,t;\theta,z) = \int_0^\xi (Z_{0z}^{(1/3)} + \Theta_{0\theta}^{(1/3)}/k)\, d\xi = -\frac{1}{2\alpha} J_1(k)\, e^z \left(1 - \frac{1}{k^2}\right)\\ \times \Big\{\theta_c(\theta)\big[\sin t + \cos t - e^{-\alpha\xi}(\sin(t-\alpha\xi) + \cos(t-\alpha\xi))\big]\\ + \theta_s(\theta)\big[\sin t - \cot t - e^{-\alpha\xi}(\sin(t-\alpha\xi) - \cos(t-\alpha\xi))\big]\Big\}.\end{aligned} \tag{B 17}$$

One can see that $|R_1^{(1/3)}| \to O(\epsilon^{1/3})$ and $\Theta_0^{(1/3)} \sim Z_0^{(1/3)} \to 0$ as $\xi \to +\infty$, in what follows, the asymptotic condition (B 13) is automatically satisfied.

Eqs. (B 16), (B 17) present the well-known solution of the linear boundary-layer problem given in term of the *differences* between viscous and inviscid velocity fields. To restore the viscous velocity field $\boldsymbol{V}$, one should take this solution, the lowest-order inviscid flow component (2.3), substitute $\xi = (k-r)/\delta$. This gives

$$\begin{aligned}U^{(1/3)} = v_1^{(1/3)},\ V^{(1/3)} = v_2^{(1/3)} + \Theta_0^{(1/3)}((k-r)/\delta,t;\theta,z),\\ W^{(1/3)} = v_3^{(1/3)} + Z_0^{(1/3)}((k-r)/\delta,t;\theta,z).\end{aligned}$$

This time-periodic solution is zero on the tank surface and rapidly converges to $\boldsymbol{v}^{(1/3)}$ away from the boundary layer. It does not contain a steady-flow component, which is expected in the second-order approximation.

B.2.2. *The $O(\epsilon^{2/3})$ component; steady streaming*

Inserting (B 16) and (B 17) into (B 11) leads to the inhomogeneous parabolic equations with respect to $\Theta_0^{(2/3)}$ and $Z_0^{(2/3)}$

$$\dot{\Theta}_0^{(2/3)} - \Theta_{0\xi\xi}^{(2/3)} = R_1^{(1/3)}\Theta_{0\xi}^{(1/3)} - \frac{\Theta_0^{(1/3)}\Theta_{0\theta}^{(1/3)}}{k} - Z_0^{(1/3)}\Theta_{0z}^{(1/3)} - \xi\bar{u}_r^{(1/3)}\Theta_{0\xi}^{(1/3)} - \frac{1}{k}\left[\bar{v}^{(1/3)}\Theta_{0\theta}^{(1/3)} + \bar{v}_\theta^{(1/3)}\Theta_0^{(1/3)}\right] - \left[\bar{w}^{(1/3)}\Theta_{0z}^{(1/3)} + \bar{v}_z^{(1/3)}Z_0^{(1/3)}\right], \quad \text{(B 18}a\text{)}$$

$$\dot{Z}_0^{(2/3)} - Z_{0\xi\xi}^{(2/3)} = R_1^{(1/3)}Z_{0\xi}^{(1/3)} - \frac{\Theta_0^{(1/3)}Z_{0\theta}^{(1/3)}}{k} - Z_0^{(1/3)}Z_{0z}^{(1/3)} - \xi\bar{u}_r^{(1/3)}Z_{0\xi}^{(1/3)} - \frac{1}{k}\left[\bar{v}^{(1/3)}Z_{0\theta}^{(1/3)} + \bar{w}_\theta^{(1/3)}\Theta_0^{(1/3)}\right] - \left[\bar{w}^{(1/3)}Z_{0z}^{(1/3)} + \bar{w}_z^{(1/3)}Z_0^{(1/3)}\right], \quad \text{(B 18}b\text{)}$$

where the right-hand sides are explicitly-given functions.

Because the steady streaming effect is formally included into the ambient flow, the time-periodic solution of (B 18) (governing the differences!) should *obligatory* decay at the infinity,

$$\Theta_0^{(2/3)}(\xi,t;\theta,z) \to 0 \ \text{ and } \ Z_0^{(2/3)}(\xi,t;\theta,z) \to 0 \ \text{ as } \ \xi \to +\infty. \qquad \text{(B 19)}$$

In addition, the second-order differences should satisfy the boundary conditions (B 12) $\Rightarrow$

$$\Theta_0^{(2/3)}(0,t;\theta,z) = -\bar{v}^{(2/3)}, \qquad \text{(B 20}a\text{)}$$

$$Z_0^{(2/3)}(0,t;\theta,z) = -\bar{w}^{(2/3)}, \qquad \text{(B 20}b\text{)}$$

where, according to (3.3), the right-hand sides include, formally, the *time-independent projections* of $\boldsymbol{w}^E = O(\epsilon^{2/3})$ on $r = k$.

When solving the *linear inhomogeneous* problem (B 18)-(B 20) with respect to the unknowns $\Theta_0^{(2/3)}$ and $Z^{(2/3)}$, we should distinguish the time-independent (steady) quantities as well as the $\cos 2t$ and $\sin 2t$ harmonics.

Huge derivations show that a unique solution exists for the $\cos 2t$ and $\sin 2t$ components. This means that these components of the difference field exist only in the boundary layer but vanish away from it.

However, considering the time-averaged (time-independent, steady) difference field yields a requirement on $\boldsymbol{w}^E$. Indeed, derivations show that the time-averaged component of (B 18), (B 19) (*without* the boundary conditions (B 20)!!!) has the following unique solution

$$\left\langle \Theta_0^{(2/3)} \right\rangle (\xi;\theta,z) = \frac{(k^2-1)J_1^2(k)}{4k^3\alpha^2} e^{-\alpha\xi+2z}\Big\{(ab-\bar{a}\bar{b}) \times \left[-\tfrac{1}{2}e^{-\alpha\xi} + (\alpha\xi-1)\sin\alpha\xi + (\alpha\xi+2)\cos\alpha\xi\right] + \left[\tfrac{1}{2}e^{-\alpha\xi} + (\alpha\xi+4)\sin\alpha\xi + (1-\alpha\xi)\cos(\alpha\xi)\right] \times \left[(a\bar{b}+\bar{a}b)\cos 2\theta + \tfrac{1}{2}(b^2+\bar{b}^2-a^2-\bar{a}^2)\sin 2\theta\right]\Big\}, \qquad \text{(B 21}a\text{)}$$

$$\left\langle Z_0^{(2/3)} \right\rangle (\xi;\theta,z) = \frac{J_1^2(k)}{8k^2\alpha^2} e^{-\alpha\xi+2z}\Big\{\tfrac{1}{2}(a^2+\bar{a}^2+b^2+\bar{b}^2) \times \left[(k^2+1)e^{-\alpha\xi} + 2[k^2(\alpha\xi+4)-\alpha\xi]\sin\alpha\xi - 2(k^2-1)(\alpha\xi-1)\cos\alpha\xi\right]$$

$$+\left[\tfrac{1}{2}(a^2+\bar{a}^2-b^2-\bar{b}^2)\cos 2\theta+(a\bar{b}+\bar{a}b)\sin 2\theta\right]$$
$$\times(k^2-1)\left(e^{-\alpha\xi}+2(\alpha\xi+4)\sin\alpha\xi+2(1-\alpha\xi)\cos\alpha\xi\right). \quad (B\,21b)$$

The time-averaging in the *remaining* boundary conditions (B 20) transforms them to

$$\left\langle \Theta_0^{(2/3)}(0,t;\theta,z)\right\rangle = -w_2^E(k,\theta,z),\quad \left\langle Z_0^{(2/3)}(0,t;\theta,z)\right\rangle = -w_3^E(k,\theta,z). \quad (B\,22)$$

Using (B 21) with $\xi=0$ derives from (B 22) the tangential boundary condition for the mean Eulerian $\boldsymbol{w}^E$:

$$w_2^E(k,\theta,z) = -\left\langle \Theta_0^{(2/3)}\right\rangle(0;\theta,z) = -\frac{3(k^2-1)J_1^2(k)}{4k^3}e^{2z}\Big\{\boxed{\underbrace{(ab-\bar{a}\bar{b})}_{\Xi}}$$
$$+(a\bar{b}+\bar{a}b)\cos 2\theta+\tfrac{1}{2}(b^2+\bar{b}^2-a^2-\bar{a}^2)\sin 2\theta\Big\}, \quad (B\,23a)$$

$$w_3^E(k,\theta,z) = -\left\langle Z_0^{(2/3)}\right\rangle(0;\theta,z) = -\frac{J_1^2(k)}{4k^2}\,e^{2z}\Big\{\boxed{\tfrac{1}{2}(a^2+\bar{a}^2+b^2+\bar{b}^2)(3k^2-1)}$$
$$+3(k^2-1)\left[\tfrac{1}{2}(a^2+\bar{a}^2-b^2-\bar{b}^2)\cos 2\theta+(a\bar{b}+\bar{a}b)\sin 2\theta\right]\Big\} \quad (B\,23b)$$

on the vertical wall.

## Appendix C. The Stokes drift in a rectangular channel

For the incompressible wave flow $\mathbf{v}$, the first-order Lagrangian displacement is $\mathbf{d}=\int\mathbf{v}\mathrm{d}t$; it is also solenoidal. The Stokes drift velocity (in the second-order approximation) equals to (see, equation (3.9))

$$\mathbf{w}^S = \frac{1}{2}\nabla\times\langle\mathbf{v}\times\mathbf{d}\rangle\,. \quad (C\,1)$$

Assume that $\mathbf{v}$ implies a three-dimensional progressive wave in the $Oy$ direction in a rectangular channel confined by the vertical walls at $x=\pm a$, the bottom $z=-h$, and the mean free surface at $z=0$. We consider the cross-sectional plane at $y=0$, which intersects the time-changing two-dimensional cross-sectional area $C(t)$ confined by the solid part (walls and bottom, $\gamma_0$), and the free-surface curve $\gamma(t)$ by $z=\zeta(x,t)$. Within the framework of the first-order (linear) approximation, $\zeta$, due to the linear kinematic boundary condition, is linked with the first-order Lagrangian displacements $\mathbf{d}$ as follows

$$z=\zeta(x,t)=d_3(x,0,0,t) \quad (C\,2)$$

(fluid particles are kept on the free surface).

We assume that $\mathbf{w}^S$, $C(t)$, and boundaries $\gamma_0$ and $\gamma(t)$ satisfy assumptions of the Stokes integration theorem. Keeping only quadratic terms and taking into account that normal velocities (and Lagrange displacements) are zero on the solid parts (walls and bottom) gives

$$M^S=\int_{\langle C\rangle}\frac{1}{2}\nabla\times\langle\mathbf{v}\times\mathbf{d}\rangle\cdot\hat{\mathbf{y}}\mathrm{d}y\mathrm{d}z=\int_{-a}^{a}\frac{1}{2}\left\langle(v_2d_3-v_3d_2)|_{z=0,y=0}\right\rangle\mathrm{d}x$$
$$=\int_{-a}^{a}\langle(v_2d_3)|_{z=0,y=0}\rangle\,\mathrm{d}x=\int_{-a}^{a}\langle(v_2)|_{z=0,y=0}\zeta\rangle\,\mathrm{d}x=\left\langle\int_{-a}^{a}\int_{-h}^{\zeta}v_2|_{y=0}\mathrm{d}z\mathrm{d}x\right\rangle. \quad (C\,3)$$

The backward reading of the derivation line (C 3) shows that, in the second-order

approximation, the mass-flux through the plane $y = 0$ due to moving free surface is the same as the Stokes mass-transport. The latter fact may be violated if there is an inflow/outflow though the vertical walls as in § 4, i.e. the first-order horizontal Lagrangian displacements are not zero, e.g., at $x = -a$. The cross-displacements cause an extra non-zero quantity of the non-Eulerian mean nature in (C 3) as it happened in (4.6).